Article:

Zheng, Y, Zhang, C, Wang, J et al. (3 more authors) (2019) Robust adhesion of droplets via heterogeneous dynamic petal effects. Journal of Colloid and Interface Science, 557. pp. 737-745. ISSN 0021-9797

https://doi.org/10.1016/j.jcis.2019.09.070

Elsevier Editorial System(tm) for Journal of Colloid and Interface Science
Manuscript Draft

Manuscript Number: JCIS-19-5022R2

Title: Robust adhesion of droplets via heterogeneous dynamic petal effects

Article Type: Full length article

Section/Category: D. Interfacial Processes, Capillarity and Wetting

Keywords: dynamic petal effect; droplet impact; asymmetric wetting; sticky superhydrophobic.

Corresponding Author: Professor Chengchun Zhang, P.h.D

Corresponding Author's Institution: Jilin University

First Author: Yihua Zheng, P.h.D

Order of Authors: Yihua Zheng, P.h.D; Chengchun Zhang, P.h.D; Jing Wang, P.h.D; Yan Liu, P.h.D; Chun Shen, P.h.D; Junfeng Yang, P.h.D

Abstract: Hypothesis
Bionics and dynamic interface wetting intensely appeal to many research communities due to their unique practical implications. The rose petals had a highly robust dynamic water-retaining capacity under heavy precipitation. We predicted that the roses became more "hydrophilic" at higher Weber numbers.

Experiments
Fresh rose petals were directly impacted by droplets, and facile artificial petal-like substrates and superhydrophobic substrates were used in the comparative analysis. The wetting dynamics of the droplet (e.g., topography, bounce dynamics, contact time, three-phase contact lines, and oscillations) were investigated when interacting with four selected target substrates.

Findings
The present work first time investigated the dynamic wetting rule of the sticky superhydrophobic substrates (SSHS). Simulated and experimental investigations confirmed that the unique coupling synergy between the pinning effect and the inhomogeneous micropapillaes resulted in lopsided contact line velocities, which remarkably suppressed the lateral oscillation and rebounding. This may be a new strategy when designing dynamic water-repellent surfaces and open a promising avenue for emerging areas such as super-efficiency energy conversion and harvesting.

*4a: Marked highlighted manuscript

Robust adhesion of droplets via heterogeneous dynamic petal effects

Yihua Zheng[a], Chengchun Zhang [a, b*], Jing Wang [c], Yan Liu[a], Chun Shen [b], Junfeng Yang [d]

[a]Key Laboratory of Bionic Engineering (Ministry of Education), Jilin University, Changchun 130022, China

[b]State Key Laboratory of Automotive Simulation and Control, Jilin University, Changchun,130022, China

[c]College of Physics, Jilin University, Changchun 130012, China

[d]School of Mechanical Engineering, University of Leeds, LS2 9JT, United Kingdom

Abstract

Hypothesis

Bionics and dynamic interface wetting intensely appeal to many research communities due to their unique practical implications. The rose petals had a highly robust dynamic water-retaining capacity under heavy precipitation. We predicted that the roses became more "hydrophilic" at higher Weber numbers.

Experiments

Fresh rose petals were directly impacted by droplets, and facile artificial petal-like substrates and superhydrophobic substrates were used in the comparative analysis. The wetting dynamics of the droplet (e.g., topography, bounce dynamics, contact time, three-phase contact lines, and oscillations) were investigated when interacting with four selected target substrates.

Findings

The present work first time investigated the dynamic wetting rule of the sticky superhydrophobic substrates (SSHS). Simulated and experimental investigations confirmed that the unique coupling synergy between the pinning effect and the inhomogeneous micropapillaes resulted in lopsided contact line velocities, which remarkably suppressed the lateral oscillation and rebounding. This may be a new strategy when designing dynamic water-repellent surfaces and open a promising avenue for emerging areas such as super-efficiency energy conversion and harvesting.

Keywords: dynamic petal effect, droplet impact, asymmetric wetting, sticky superhydrophobic

1. Introduction

Rain droplets on lotus leaves may be less striking than rain droplets on rose petals. Water droplets can attach to rose petals without rolling off, even at great tilt angles. However, water droplets cannot remain on lotus leaves after a rain. The “lotus effect” is synonymous with superhydrophobicity, and a superhydrophobic surface(SHS) exhibits a static apparent contact angle (CA, θ) of greater than 150° with a very low contact angle hysteresis (CAH, θ_{CAH})[1–4]. Interestingly, rose petals can exhibit an extremely high CA similar to that of the “lotus effect”, but with high CAH (Fig. 1a)[5]. This "sticky superhydrophobic” substrate (SSHS) phenomenon known as the "petal effect" was first proposed by Jiang et al.[6] and has since drawn much research attention due to its widespread use in emerging fields such as self-cleaning[7], droplet transfer, transportation[8], biochemical separation, and energy harvesting[9,10]. In addition, studying the dynamic wetting mechanism of an SSHS provides information for enhancing functional surface designs.

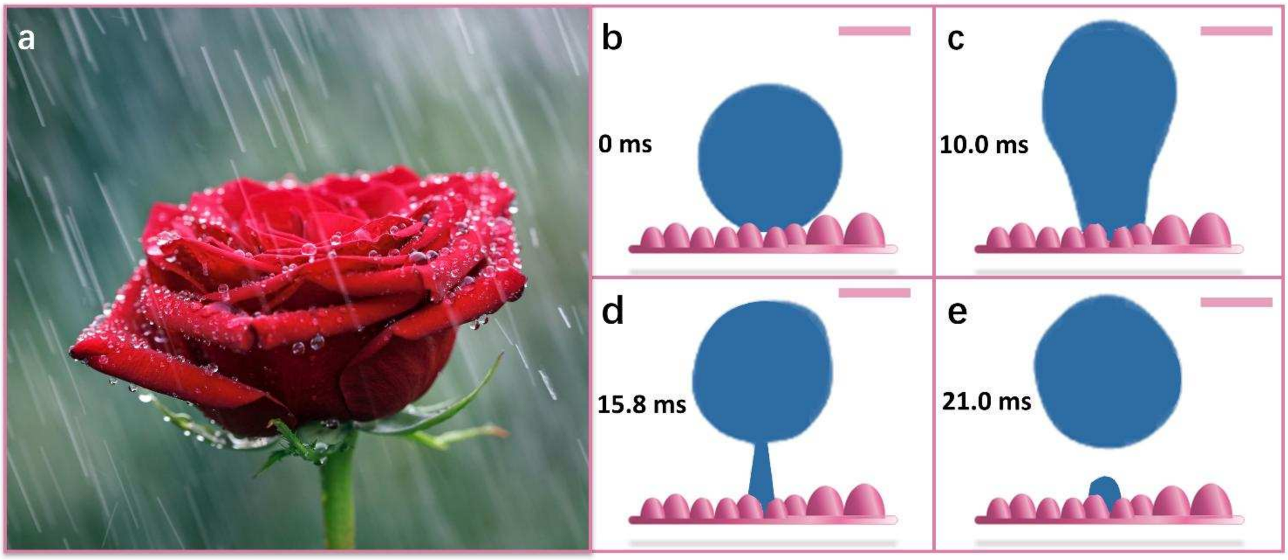

Fig. 1 Dynamic wetting phenomenon on rose petals. **(a)** Retention of spherelike droplets on rose petals in the rain. **(b-e)** Schematic diagram of the interfacial process of a droplet impacting a rose petal at low-impact velocities. The scale bar=1 mm.

Generally, the static-wetting state of rough surfaces can be explained by the classical wetting theory of Cassie-Baxter[11] and Wenzel[12]. In the Cassie-Baxter model, the rough solid surface is completely filled with liquid, resulting in high water adhesion. However, entrapped air is observed in the Wenzel model, which is attributed to hydrophobicity[13]. The superhydrophobicity exhibited on the lotus leaf results from the combination of convex epidermal cells and extremely low-density biowax layers[14]. The lotus effect should be governed by the idealized Cassie-Baxter model. For the lotus effect, research on fabricating and characterizing biomimetic surfaces is trending, both theoretically and experimentally[15–21]. In contrast, few in-depth studies have examined the petal effect; thus, the accurate mechanism of the petal effect wetting behavior remains unclear[22]. Nonetheless, the Cassie-Baxter and Wenzel models are used by most scientists to explain wettability at the interface. Adhesion of water droplets to rose petals has been attributed to the Wenzel state based on the geometric parameters of the rose petal surface determined for both biological and artificial samples. These parameters include the diameter, spacing and secondary nanostructure of the micropapillae[23](Fig. 1b-e). In contrast, the opposite conclusion has also been suggested, in that the petal's microstructure is considered to benefit adhesion, but this conclusion cannot be explained by the classic Cassie-Baxter wetting theory[24]. Thus, the rose petal wetting mechanism seems puzzling. S. Yang et al.[25] observed that the interaction between droplets and rose petals was completely in accordance with the Wenzel state, and these authors found no air cushion using micro computed tomography. Visualization technology has been developed, which has facilitated analyzing this mechanism. Optical microscopy observations using micron-scale resolution have recently shown that the wetting behavior of droplets on rose petals is unstable because gas moves slowly from the space over the liquid, thus altering the wetting state. This is a mutual transformation from the Cassie and Wenzel states[26]. This contradictory conclusion was likely reached because dynamic observations were applied to the latter; that is, the movable air cushion disappeared after connecting to the atmosphere, resulting in continuous wetting at the three-phase contact line (TCL).

Thus, the static-wetting mechanism of the petal effect remains unclear, and determining its precise dynamic wetting process is challenging. Experiments and simulations in which droplets impact the substrate have long been used to investigate the dynamic wettability of natural, artificial and chemically heterogeneous surfaces[27]. To our knowledge, previous investigations of the substrate's configuration after being impacted by the droplet mainly included liquid film[28], superhydrophilicity[29], hydrophobicity[30], superhydrophobicity[31], elastic superhydrophobicity[32,33], and vibrating superhydrophobicity[34]; however, no reports regarding droplet impact on SSH surfaces (the petal effect) have been published. Li et al.[35] reported the dynamic wetting characteristics of water droplets on various substrate configurations at CA = 160°, 154°, 153°, 122°, 124°, and 119°. Shen et al.[36] verified that a relationship exists between the trapped air and the interface adhesion when a droplet impacts a sticky hydrophobic substrate. In the two aforementioned studies, the droplets were released from the same height as that impacting the substrate, which was insufficient to summarize the rules of dynamic wetting on sticky superhydrophobic surfaces.

This paper describes the dynamic wetting rule on a SSHS (i.e., the petal effect) by comparing the wetting state on a superhydrophobic surface. The quantitative (experiments) and qualitative (simulations) investigation confirm that the dynamic unbalance wetting mechanism of the petal effect is due to the coupling of the lateral interaction of the droplets with the pinning effect, thus providing novel insights into why rose petals can retain water droplets and new rational guidelines for wetting functional surface design.

2. Experimental materials and methods

2.1 Surface fabrication and characterization

To capture the commonality of droplet dynamics on the SSHS, three target substrates were fabricated, including the rose petal surface (RPS) and engineering sticky superhydrophobic surfaces (SSHS-1 and SSHS-2). Besides, the superhydrophobic surface (SHS) is used for comparative verification.

2.1.1 Rose petal surface (RPS)

A fresh red rose was purchased from a flower market (Changchun, China), and a piece of the rose petal (15 mm × 1.5 mm) was fixed to a glass sheet which was neither cleaned nor altered.

2.1.2 Sticky superhydrophobic surface (SSHS)

We replicated the surface (SSHS-1) invented by Chen et al.[37], with some modifications to the chemical reactions. One-millimeter-thick zinc foil was ultrasonically cleaned in acetone and deionized water. The zinc foil was etched in hydrochloric acid for 15 seconds, then washed thoroughly in deionized water. Next, the zinc foil was etched in hydrochloric acid for 15 s, then immersed in 0.01 mol/L $CuSO_4 \cdot H_2O$ for 12 minutes, thoroughly washed again in deionized water, and immersed in 0.005 mol/L $CH_3(CH_2)_{16}COOH$ for 30 minutes. We also established a micron-scale with arrays on paraffin with low surface energies (SSHS-2) for comparison. (S1.2, Supplementary Information).

2.1.3 Superhydrophobic surface (SHS)

The 2-mm-thick square copper plate was etched in hydrochloric and sanding with sandpaper then treated with 1H,1H,2H,2H-perfluorodecyl trichlorosilane (Aladdin, Inc., China) via chemical vapour deposition.

2.1.4 Surface characterization

All characterization tests were performed indoors at 25℃. The surface morphology was characterized by scanning electron microscopy (SEM; EVO MA 25/LS, ZEISS, Inc., Germany) with 20-kV accelerating voltage and a three-position ultra-depth microscope (Smartzoom 5, ZEISS, Inc., Germany). The apparent contact angles were measured using a contact angle meter (DSA 22 KRUSS, Germany), wherein the water droplet volume was 4 μL.

2.1.5 Experimental apparatus and image analysis

To analyze the dynamic wetting behavior of the droplets, an experimental system was established to observe and record the droplet impacting the substrate (Fig. S1 in Supplementary Information). This system generates the water droplets (2.14±0.01 mm) using a 0.24-mm metal needle and a syringe driven by a microstepping motor. Using another microstepper motor, the droplet-to-substrate distance (H) can be varied, resulting in speeds of v=0.308–1.128 m/s. The resulting corresponding dimensionless numbers are the Weber number $W_e=\rho v^2 D_0/\gamma$= 4–50, capillary number $C_a=\mu v/\gamma$= $(4–16)\times10^{-3}$, Reynolds number $R_e=\rho v D_0/\mu$= 866–3120, and Ohnesorge number $O_h=\mu/(\rho\gamma D_0)^{1/2}$= 2×10^{-3}, with a density of ρ=997 $Kg\cdot m^{-3}$, surface tension of $\gamma=72\times10^{-3}$ N/m, and dynamic viscosity of $\mu=0.89\times10^{-3}$ Pa·s, which are the water's physical parameters.

2.1.6 Simulations

Qualitative simulation analysis was performed via the lattice Boltzmann method(the D3Q9 grid) [38,39].

63
64
65

3. Results and discussion

3.1 Morphology and wettability of the target substrates

Fig. 2 illustrates the morphology and adhesive states of the selected substrates (RPS, SSHS-1, SSHS-2 and SHS). The RPS could be visually characterized by a three-position ultra-depth microscope at 1000× magnification (Fig. 2a). The irregular array consisted of micropapillaes averaging 9±2 μm high and 19±2 μm in diameter (similar to previous studies[6,40]), which were semiautomatically obtained from the written code in MATLAB and the open-source software ImageJ by analyzing the selected images. The inset plots in Fig. 2a illustrate that the CA of the RPS was 154° ±2°, and a 4-μL droplet could adhere to the surface with a tilt angle of 180°. Similar wetting states also occur on sticky superhydrophobic zinc foils fabricated by chemical etching. The insets in Fig. 2c show that the CA of the SSHS-1 is 157°±2°, and it exhibited high adhesion. Fig. 2d shows the SHS with CA=153°±2° and θ_{CAH}=3°±1°, indicating a typical lotus effect phenomenon, which is consistent with previous studies[41,42].The microstructures in Fig. 2e–g are SSHS-2, which are manufactured by rapidly peeling off the copper mesh that was tightly attached to the solidified paraffin and the colored box indicates the corresponding selected area. The inset plot in Fig. 2e likewise shows a similar petal effect phenomenon, indicating CA=156°±2° with a large adhesive force. We established a diagrammatic sketch of a typical SSHS-2 microstructure (Fig. 2h), in which the corresponding statistical geometric parameters of the typical microstructures were short-side length: a=85±2 μm, long-side length: b=220±2 μm, width: w=50±2 μm, and height: h=50±2 μm.

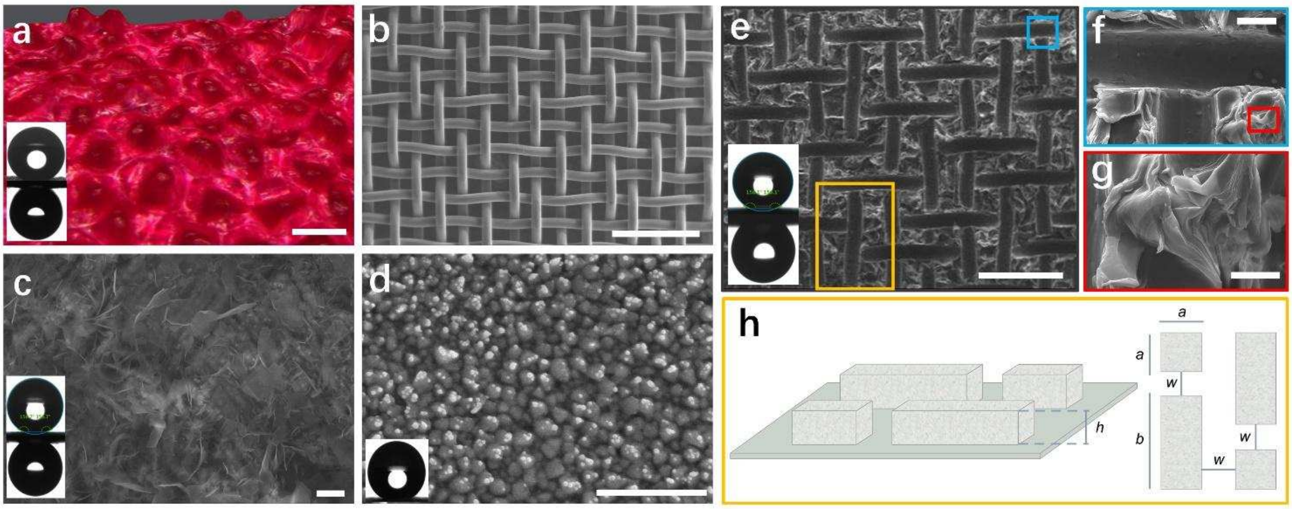

Fig. 2 Characterization of the static wettabilities of (a) RPS, (b) 200-mesh copper mesh, (c) SSHS-1, (d) SHS and (e–h) SSHS-2. **(a)** Image of a fresh rose petal captured by a 3D super depth-of-field microscope at 1000× magnification (scale bar=25 μm). The darker red indicates the top of the mastoid, while the relatively low area is shown in light red. The RPS exhibited a petal effect phenomenon with CA=154°±2° and high adhesion, as illustrated in the insets. **(b)** SEM image of the 200-mesh copper mesh (scale bar=500 μm). **(c)** SEM image of SSHS-1 (scale bar=4 μm). The insets indicate that the CA=156°±2° with the high adhesive phenomenon. **(d)** SEM image of a superhydrophobic surface with CA=153°±2° (see inset). The scale bar=500 nm. **(e)** Regular array of paraffin cubes with the same spacing and height. The insets indicate that CA=157°±2° with markedly high adhesive behavior (scale bar=300 μm). **(f)** T-shaped paraffin microstructure (blue boxes). Compared with the top of the raised paraffin square column, the trace of the single copper wire was almost smooth at the same magnification factor. (scale bar=40 μm) **(g)** The top of the raised paraffin square column is shown in red boxes. **(h)** Schematic diagram of a typical microstructure model (orange boxes). The microstructure dimensional parameters were a=85±2 μm, b=220±2 μm, w=50±2 μm, and h=50±2 μm (scale bar =20 μm).

3.2 Qualitative and quantitative analysis of Non-uniform lateral interaction on the SSHS

Simulations are performed to qualitatively explain the effect of the unbalanced Young's force dF_t on the wettability of the interface. The micropapillaes and droplets are of the same order of magnitude to facilitate intuitive analysis (Fig. 3a).Two-phase fluid dynamics equations are solved using the D3Q19 grid based on a lattice Boltzmann algorithm[38,39]. The micropapillaes of the RPS are arranged in regular arrays during a simulation. In addition, the larger micropapillaes (height =0.4 mm with diameter =0.4 mm) are configured with a CA of 150° to counteract the superhydrophobicity, whereas the CA of the secondary micropapillaes (height =0.2 mm with diameter =0.2 mm) is configured for 110°. The high-impact velocity droplets oscillated randomly and finally adhered to the rose petals; otherwise, the droplets have bounced at a low-impact speed. The droplets tend to adhere to the petals with the increasing Weber numbers, as reflected in the residual droplets (red dotted circle in Fig. 3e). The additional viscous dissipation during the droplet-petal interaction in the high Weber number state is attributed to cooperation between the irregular morphology[43] (micropapillaes, Fig. 2a) and the sticky superhydrophobicity of the rose petals. Anomalous droplet formation was initialized during the spreading phase; however, the asymmetrical speed of the moving contact line was evident in the receding phase from a two-dimensional perspective in the schematic (Fig. 3 a-d). The lateral rebounding of a droplet can be manipulated because of the uneven gradient on the textured surface[44] and the unbalanced Young's force expressed as

$$\mathrm{dF} = \sigma \left| \cos\theta_{\mathrm{Rt}} - \cos\theta_{\mathrm{Lt}} \right| \mathrm{ds}, \quad (1)$$

where $\cos\theta_{\mathrm{Rt}}$ and $\cos\theta_{\mathrm{Lt}}$ are the apparent contact angles of the right and left sides(Fig. 3 a-d), respectively, which were evaluated instantaneously by image analysis. $\mathrm{d_s}$ is the differential of the moving contact line, and dF is the transient unbalanced Young's force, which resists the inertia of the droplet. Thus, as $\left|\cos\theta_{\mathrm{Rt}} - \cos\theta_{\mathrm{Lt}}\right|$ increases (the droplet is more distorted), $\mathrm{F_t}$ also increases, resulting in a more "hydrophilic" substrate, which is consistent with that shown in Fig. 3e. Here, the effective unbalanced Young's force ($\mathrm{F_e}$) can be simplified as

$$\Delta \propto \left|\cos\theta_{\mathrm{Rt}} - \cos\theta_{\mathrm{Lt}}\right| \propto \frac{1}{5}(\lg\left|\theta_{\mathrm{Rt}} - \theta_{\mathrm{Lt}}\right|) \quad (2)$$

via analyzing the simulations. Δ contains a constant $\frac{1}{5}$, so that Δ is in the same order of magnitude as the quantitative result, which is advantageous for comparison verification.

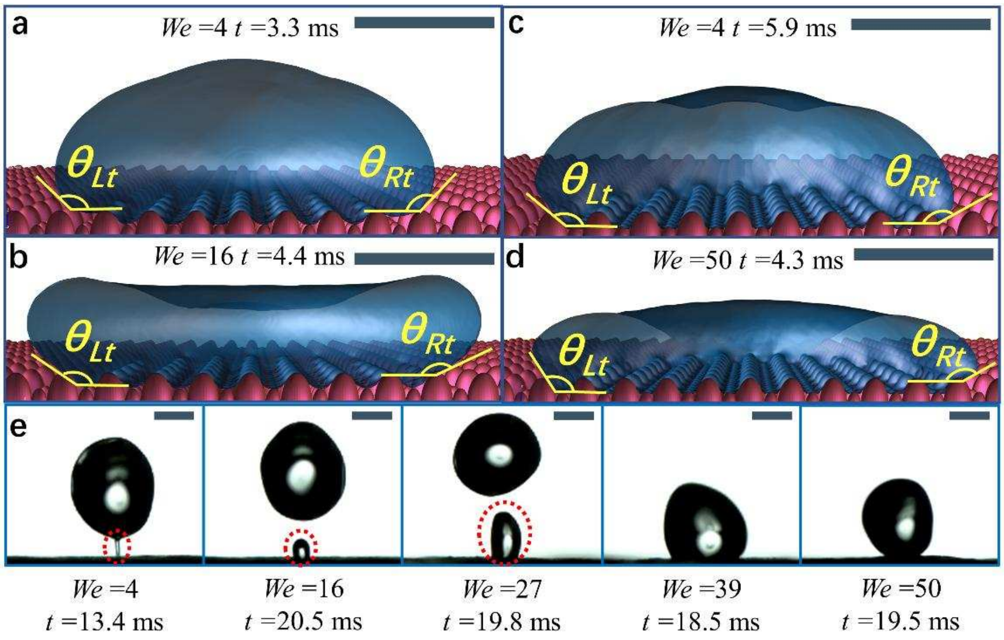

Fig. 3 Simulated and experimental analysis and verification of the unbalanced Young's force caused by the SSHS. **(a)-(d)** Simulation analysis of droplets are observed to be in the most laterally unbalanced. Unbalanced droplet morphology due to irregular micropapillaes in the receding phase. Consequently, the Young's force increases, causing additional energy dissipation. The results of the simulation show that the difference between $\cos\theta_{\mathrm{Lt}}$ and $\cos\theta_{\mathrm{Rt}}$ is more significant as the Weber number increases, so higher F_e eventually lead to droplets adhesion. The scale bar= 1.8 mm. **(e)** The quantitative similarity of various morphologies of pinging tiny droplets (red dotted circle) on a rose petal as the Weber number increased. The rose petals became more "hydrophilic". The scale bar= 1 mm.

However, the aforementioned effective unbalanced Young's force F_e is transient and difficult to quantify via experiments. Thus, the dimensionless size of the residual droplets, $\lambda = D_r / D_0$, is used to investigate the extent of the dynamic petal effect due to the intuitive result of the dynamic petal effect is reflected in the residual moisture on the RPS, as shown in Fig. 3e. These retained liquids on the RPS are essentially caused by varying degrees of the Cassie-to-Wenzel transition[11,12] which can be regarded as the partial wetting state. This partial wetting state is mainly governed by the effective water hammer pressure verified by Tao et al[45],

$$P_{EWH} = k\rho Cv, \tag{3}$$

where C is the speed of sound in water, and k is the fitting parameter of the corresponding experiment. Herein, $v \propto We^{0.5}$ and then $P_{EWH} \propto \alpha We^{0.5}$,where $\alpha = k\rho C$ .In this case, we assumed that that dF_t is in a two-dimensional environment, thus dF_t and λ are in the same dimension and related. Together with Eq. (1-3), the quantitative estimation of dynamic petal effect of RPS would yield $dF_t \propto (\zeta = \alpha We^{\beta\lambda}) \propto \Delta \propto \alpha We^{\gamma}$ .Thereby,

$$\zeta = 0.0366(\frac{\rho v^2 D_0}{\gamma})^{0.633}, \quad (3)$$

where $4 < W_e = \frac{\rho v^2 D_0}{\gamma} < 27$ .Eq. (3) are satisfied in our experiments (Fig. 3e and Fig. 4a): the dynamic water-repellency of the SSHS is only closely related to the impact velocity of the droplets (v). The limit (W_e<4) was considered as the inconspicuous dynamic petal effect regime, while the critical total wetting state occurs when W_e>27. Furthermore, the simulation results (Fig. 3 a-d and Fig. 4b-d) qualitatively reveal the adhesion water caused by the lateral effect of the droplets of the SSHS in this study. Thus, the aforementioned effective unbalanced Young's force F_t would yield

$$\Delta = 0.0259(\frac{\rho v^2 D_0}{\gamma})^{0.638}. \quad (4)$$

Herein, $4 < W_e = \frac{\rho v^2 D_0}{\gamma} < 50$ .The results of the simulation (the blue line in Fig. 4a) satisfactorily confirm the positive effect of the lateral effect on droplet adhesion. The RPS—with its unique asymmetric natural sticky superhydrophobic, resulting in solid edges with discontinuous physical properties (e.g. wettability) that directly affect the receding speed of the three-phase contact line, which is striking at higher at high Weber numbers. As shown in yellow dotted circles in Fig. 4d, significant asymmetric receding line velocities and morphology are observed on both sides of the droplet, in contrast, symmetrical edge velocities occur at low Weber numbers(Fig. 4 b-c). Qualitatively, the synergy of the multiple lateral asymmetric effects and sticky will make the SSHS more sticky and "hydrophilic" at high droplet impinging velocities regime (see the insets in Fig. 4).

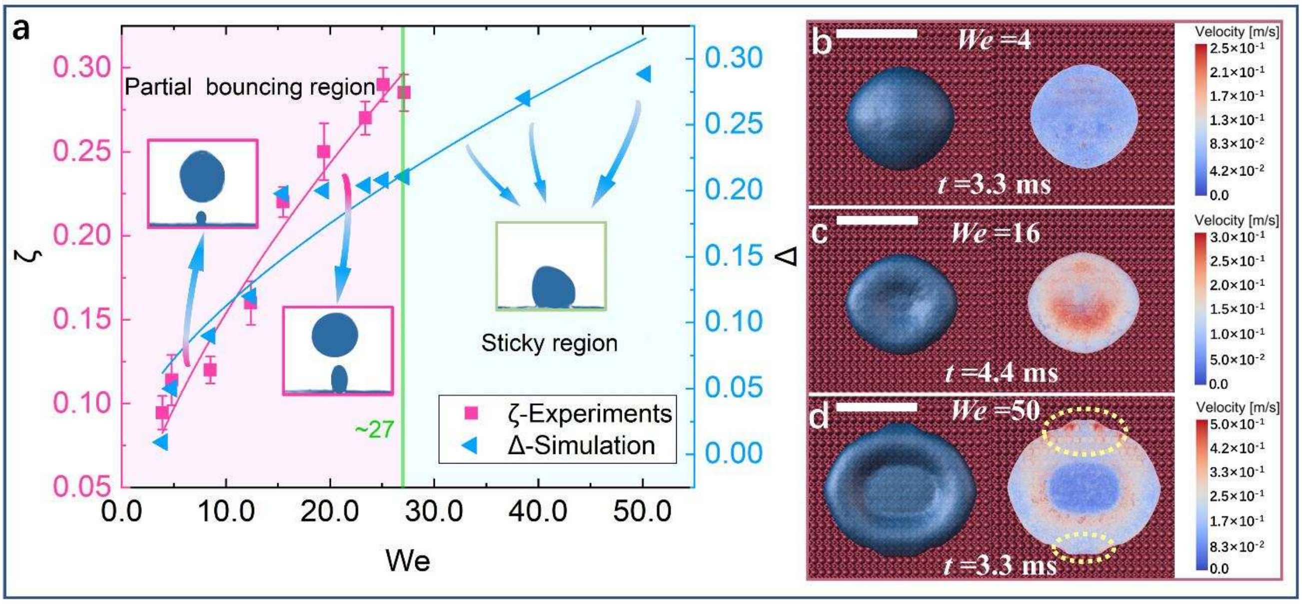

Fig. 4 Quantitative and qualitative comparisons of the effects of multiple lateral pinning on the RPS's wetting characteristics. **(a)** Investigations of the correlation between lateral effects and sticky adhesion on the SSHS. The insets show the extent of the dynamic petal effect, from pinning tiny droplets (partial rebound, lilac region) to no bouncing sticky region (light green area) as the Weber number increases. Satisfactory qualitative similarities are revealed in experimental and numerical results (purple and blue fitted line)**.** The critical of the partial bouncing region and sticky region is W_e = 27 (green line). **(b)-(d)** The simulated velocity field as the droplets develop to their most asymmetrical morphology. Axisymmetric droplet morphology occurs under the low Weber number regime (W_e = 4), but note that the higher impinging velocities (corresponding to W_e = 50) result in remarkable unbalanced receding velocities (yellow dotted circle).Both versions of the investigation confirmed the same characteristic that asymmetric interactions caused by high weber number reduce the possibility of droplet bouncing. The scale bar=4 mm.

3.3 Droplet bounce dynamics

In order to verify the above-mentioned theory, three SSHSs (the RPS, SSHS-1 and SSHS-2) and a SHS were selected as the target substrates. When a droplet hits a rough solid surface, it may bounce or stick, after undergoing the spreading and receding stages. The interfacial behavior of the droplets corresponds to the hydrophobicity (e.g., CA and CAH) of the substrate and is significantly affected by the wettability (e.g., high adhesion) of the interface[27]. We examined the droplet impact on the four aforementioned surfaces. For droplets, the low-impact velocity resulted in a low kinetic energy level. Fig. 5 illustrates the dynamic wetting process of the droplets on RPS, SSHS-1, SSHS-2 and SHS at a very low Weber number (W_e= 4, corresponding to v=0.362±0.001 m/s; see also Supplementary Movie S1). Droplets with sufficient kinetic energy can generally bounce off sticky superhydrophobic substrates at a very low Weber number, W_e= 4 (Fig. 5 a–c). Partial pinning occurred at the bottom of the droplet resulting in a slightly longer contact time than that on the SHS (see S3 in Supplementary Information for more details). The bounce of the drop was partially inhibited when the droplet impacted the sticky superhydrophobic substrate compared with that on the superhydrophobic substrate under the corresponding impacting velocity.

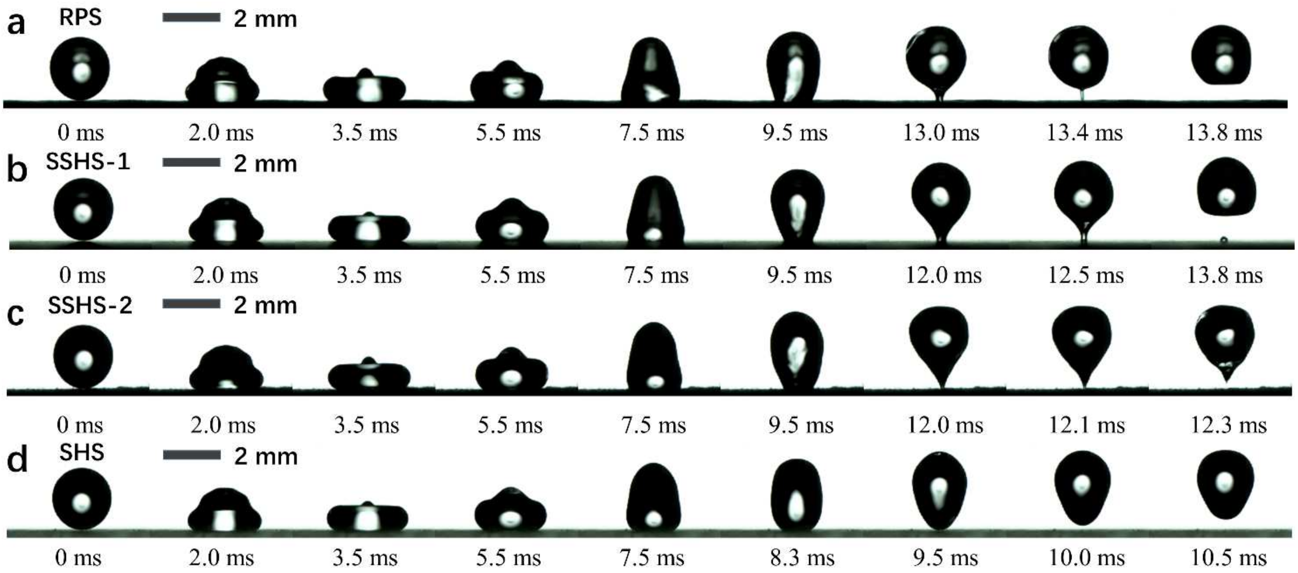

Fig. 5 Snapshots of the droplets' dynamic behavior on RPS, SSHS-1, SSHS-2 and SHS (W_e= 4, corresponding to v=0.362±0.001 m/s). **(a–c)** Time evolution of an impacting droplet on RPS, SSHS-1, SSHS-2, respectively. The droplet morphology becomes asymmetrical during the receding phase. Droplets can still rebound, but the substrates exhibit some viscosity. **(d)** Impact phase diagram of a droplet impacting the SHS. The droplet lifts off the substrate with less contact time and remains more symmetric compared with that on the aforementioned substrates. Supplementary Movie S1 provides more details. The scale bar=2 mm.

As the Weber number increases slightly (W_e= 16, corresponding to v=0.723±0.001 m/s), the SSHS plays a more vital role in the droplets' dynamic behavior than does the SSH. Detaching the droplet from the SSHS was more difficult and differed greatly from its interaction on the SHS (Fig. 6; Supplementary Movie S2). The droplet morphology on all target substrates was almost synchronous during the spreading phase (0 ms < t < 3.5 ms) and was independent of the target substrate's wettability and impact velocity, which is consistent with previous studies[33,36,46]. For the RPS, the geometric center of the droplet changed and gradually moved away from the axis of symmetry, indicating more sensitivity to the impact velocity of the droplet after 3.5 ms than at the We of 4 (Fig. 5 a and Fig. 6a). Thus, the droplet exhibited difficulty in rebounding completely, even with a higher initial kinetic energy, as illustrated by the residual secondary droplets on the sticky substrate (blue and green dotted circles in Fig. 6a, see also S4 in Supplementary Information). Interestingly, similar wetting phenomena were observed on both SSHS-1 and SSHS-2 (Fig. 6b–c). One droplet was difficult to lift off and was even pinned to the substrate (red dotted circle in Fig. 6c). Instead, the droplet lifted off from the SHS quickly after undergoing a spreading and retracting phase similar to that of the above corresponding testing condition. We confirmed that the dynamic response of the droplets is critical to wetting the SSHS interface during the receding phase when $4 \leq W_e \leq 16$.

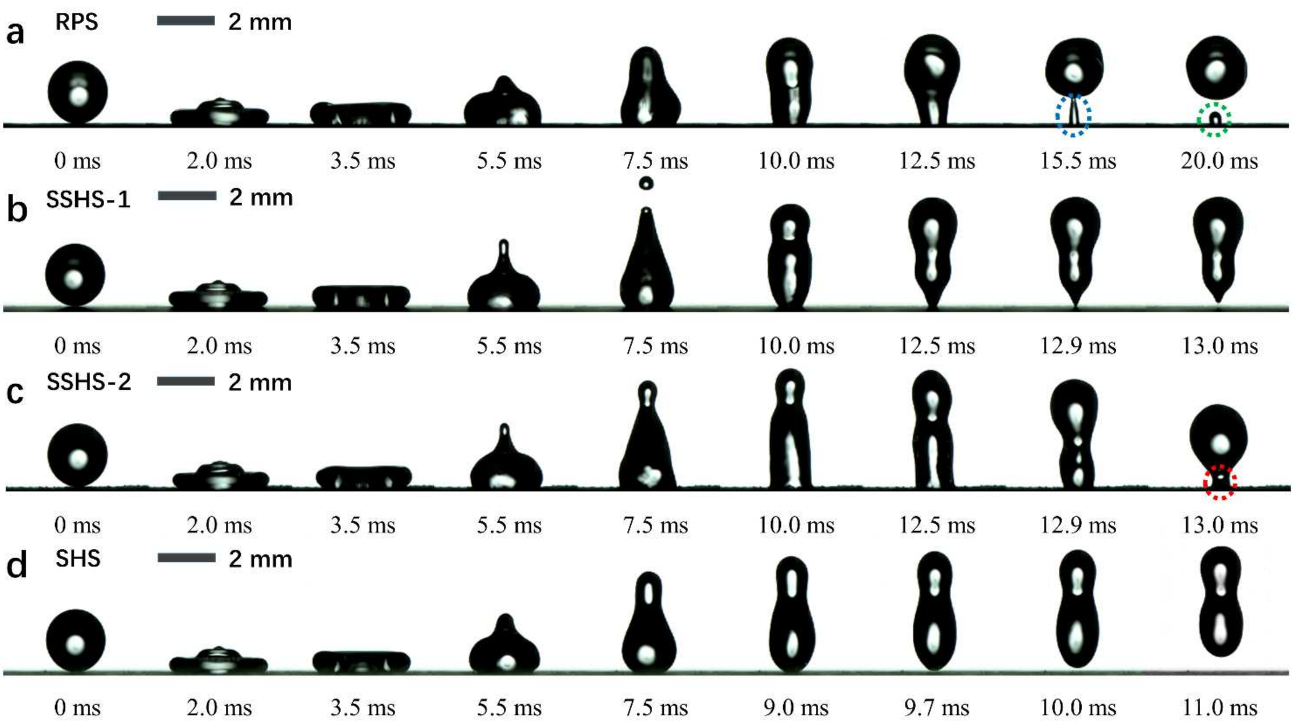

Fig. 6 Sequential snapshots of the droplets' dynamic behaviors on the RPS, SSHS-1, SSHS-2 and SHS (W_e=16, corresponding to v=0.723±0.001 m/s). **(a)** Impact phase diagram of a droplet impacting the RPS. Note that this droplet was observed to be extremely asymmetric at t=5.5 ms. During the

rebound phase, the liquid bridge (blue circle) is captured between the ejecting droplet and the substrate. A residual secondary droplet is shown in the green circle. **(b)** Drop impacting the SSHS-1 with a tiny droplet ejecting at t=7.5 ms. **(c)** A droplet is completely trapped on the SSHS-2. A larger liquid bridge is observed at the interface and is circled in red. **(d)** Sequential phase diagram of a droplet impacting the SHS. Almost no adhesion was observed (Supplementary Movie S2). The scale bar=4 mm.

Interestingly, as we predicted, the spreading phase of the droplets was also affected by the substrate configuration, such as in the receding phase when the impact velocity was high (W_e=50, corresponding to v=1.304±0.001 m/s), which appears to be inconsistent with previous studies. In the present study, the surface tension and viscosity of the water were constant and were factors that inhibited the droplet from receding[47]. Fig. 7 shows the dynamic process of the droplet impacting the RPS and SSHS-2 (Supplementary Movie S3). The droplet morphology is extremely asynchronized during the spreading phase after t=2 ms. In addition, the droplet showed a maximum twist compared with all previous test conditions and exhibited a surprisingly dF and could not to lift off the substrate (Fig. 7a). Previously, we confirmed that droplets are more likely to adhere at high Weber numbers, but did not qualitatively clarify the droplets' reciprocating oscillation on the RPS. Once the de-pinning effect is initialized (red box in Fig. 7a), the de-pinning force for the moment, including the inward and upward forces, will be activated (green box in Fig. 7a). The mechanism of the corresponding state can be qualitatively explained by the blue box in Fig. 7b and the green box in Fig. 7c, respectively. Note that dF, with both upward and inward vectors, drives the leftmost liquid to hit those adjacent portions with lower receding velocities, instead, the de-pinning does not occur on the rightmost, thus the droplet exhibits unbalanced and eventually cause reciprocating oscillation of a droplet on a rose petal. The free liquid-gas interface adjacent to the petal is pinned again, causing multiple viscous energy dissipation, and the petal eventually becomes more "hydrophilic".

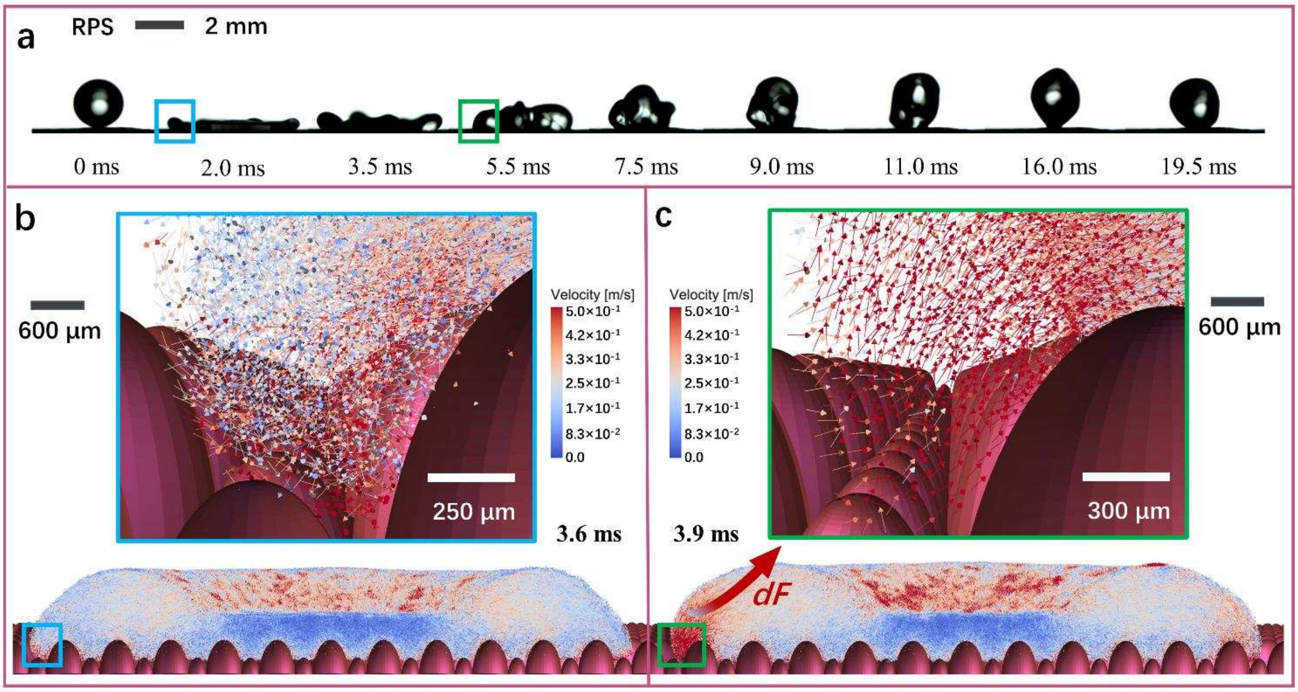

Fig. 7 Impact of droplets on the RPS at high velocities (W_e=50, corresponding to v=1.304±0.001 m/s). **(a)** A droplet impacts the RPS, exhibiting a sharp anisotropic vibration that prevents it from bouncing off the substrate. As we predicted, the non-negligible unbalanced Young's force increases with higher Weber number regime due to the strong asymmetrical solid-liquid interaction (See Supplementary Movie S3 for more details). The scale bar=2 mm. **(b)-(c)** Side-view snapshots of force analysis of the de-pinning procedure (3.6-3.9 ms). The velocity vectors of the particles are represented by arrows, and the zoomed area (blue box, the scale bar=250 µm) indicates that the high inward velocities vector only occurs at the wall before de-pinning. Subsequently, the leftmost particles have both inward and upward velocity vectors, which then impact adjacent low-velocity portions, causing unbalanced oscillations and additional energy dissipation, ultimately depleting the energy of the upward impact of the droplets(green box, the scale bar=300 µm).

3.4 Unique mechanism for suppressing oscillation

The TCL is always accompanied by the whole process of solid-liquid interaction, which does not merely increase the effective interfacial friction but also suppresses the bouncing droplets[48]. The size of the annular TCL can be quantified by the length of the horizontally overlapping lines (D_h). As a function of the time scale, D_h was normalized by the initial diameter D_0 (Fig. 8). A droplet can bounce from both a sticky superhydrophobic substrate and a superhydrophobic substrate, which was reflected in the similarity of the TCL when the droplet underwent a symmetrically evolved interaction with the substrate (W_e =4, Fig. 8 a). The TCL evolved as a function of time scales, and the peaks of these curves correspond to the droplet's maximum spreading diameter (D_{max}) when it impacted the four selected substrates. The maximum spreading factor β_{max}= $(D_{max}/D_0) \sim W_e^{0.25}$ =1.405 is a critical parameter for evaluating inertia-dominated wetting kinetics based on mass conservation, which is consistent with the conclusions drawn by Clanet et al.[49]. This also indicates that the droplet's dynamic response is independent of the substrate configuration and remains dominated by inertia within a low Weber number regimen. For the higher W_e=50, the effect of the substrate configuration on the impact dynamics of the droplets was more effective. All droplets accomplished the spreading process in 3 ms, then experienced a more time-consuming receding phase (Fig. 8b). The distinguishable curves indicate that the droplet morphology was more sensitive to the substrate configuration than that within the high Weber number regimen. We also noticed that the rose petals exhibited the strongest robust liquid viscous effect[48] compared with the other three target substrates during the solid-liquid interaction process. In addition, the comparative analysis indicated that the droplet spreading was strongly suppressed at the liquid-petal interface, and the excess restoring force (reflected in the viscosity of the droplets) was transformed into the surface energy of the irregular twisting droplet (t =7.5 ms in Fig. 7a). The irregular droplet twist caused the surface energy to be consumed by both the viscosity of the droplet and the partial pinning effect of the petals based on the energy conservation argument, eventually leading to droplet adhesion. Conversely, the spreading and retraction of the droplets were maximized because the SHS exhibited the lowest contact angle hysteresis among all selected substrates[2,3]. Analysis of the contact line showed that this twist was relatively stable, while the other three selected substrates exhibited larger fluctuations.

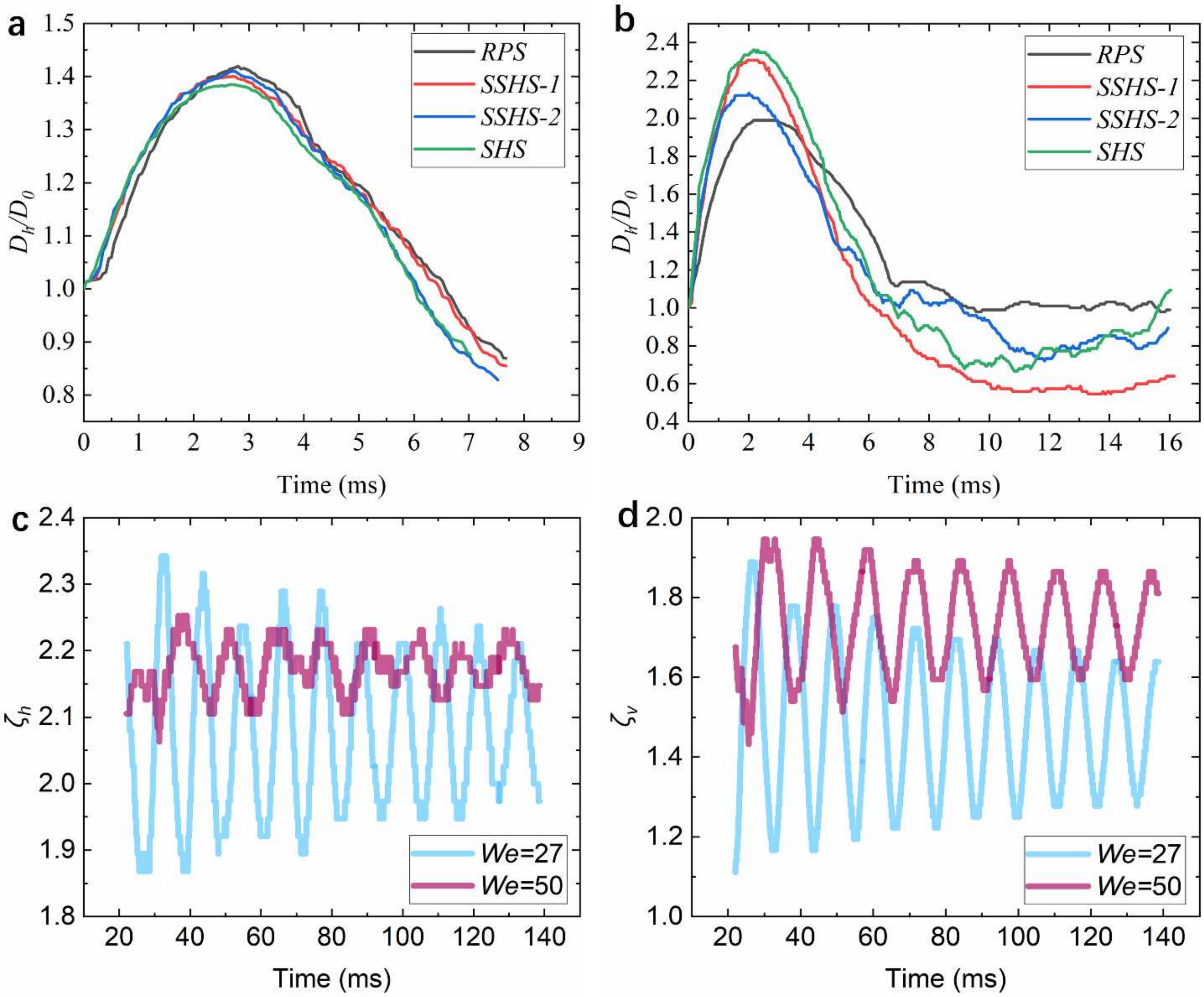

Fig. 8 Transient contact diameter of the droplet impacting the four substrates at **(a)** W_e=4 and **(b)** W_e=50. The difference was not significant under the low Weber number regimen. Nevertheless, the substrate configuration dominated the droplet topography at W_e=50. **(c)** Comparative analysis of the horizontal flatness factor, ζ_h, under moderate (W_e=27) and high (W_e=50) Weber numbers. The lateral droplet response was consistent in the latter case. **(d)** Comparative analysis of the vertical flatness factor, ζ_v, under moderate (W_e=27) and high (W_e=50) Weber numbers. Unexpectedly, the high-impact velocity of a droplet led to a lower amplitude.

Attenuation of the droplet oscillation is similar to the underdamped harmonic oscillator, which has the characteristics of a vibration system composed of a spring, damping, and mass with a certain degree of freedom[33]. To quantify this oscillation, the oscillation frequencies were analyzed in the horizontal ($f_h = 1/T_h = \omega_h/2\pi$) and vertical ($f_v = 1/T_v = \omega_h/2\pi$) directions using the fast Fourier transform algorithm[50,51] in MATLAB. Under the high Weber numbers, the droplet oscillation frequency was lower than that under the moderate-impact velocity condition, where f_{h50} = 80 Hz < f_{h27} = 93 Hz and f_{vh50} = 76 Hz < f_{v27} = 90 Hz (the frequency of a free-oscillating droplet: f =109 Hz[52]). Thus, the lower frequency and smaller amplitude of the droplet oscillations reveal that more energy is dissipated by the viscous force at high-impact velocities. Additionally, mutations in the degree of freedom of the droplet-spring system due to pinning/depinning can severely inhibit lateral but not vertical droplet oscillations during the retraction process; thus, the lower part of the droplet will again collide with the petal, causing multiple surface energy dissipation as demonstrated in Fig. 7. Artificial SSHSs (e.g., SSHS-1, SSHS-2) are more isotropic with respect to the rose petals but can also become more "hydrophilic" under high Weber numbers. In addition, the underdamped harmonic oscillator, especially in the horizontal direction (Fig. 8a), are highly efficient on the RPS. The pinning effect of the high regimen experienced random oscillation in an underdamped manner on the rose petals. The flatness factor, $\zeta_h = D_h/D_0$, and the dimensionless vertical dimension of the droplet, $\zeta_v = D_v/D_0$, were defined to investigate the degree of oscillation. Furthermore, we analyzed the oscillation phenomenon of the depositional droplet under moderate (W_e =27) and high (W_e =50) Weber numbers as denoted in Fig. 8, resulting in greater damping and droplet stiffness at W_e =50. The increased velocity appeared to attenuate the oscillation amplitude faster than did the collision of a lower velocity droplet on the same petal, indicating a higher effective damping coefficient.

4. Conclusions

There seems to be no consensus on the static petal effects[22–24,26] and a large amount of the previous studies have mainly focused on the wettability of superhydrophobic surfaces[15–21,42].These all determine that the dynamic petal effects are still far from being fully understood yet. We systematically investigated the impact dynamics of droplets on the interfaces of rose petals, imitation rose petals and SHS. Spherical droplet retention is attributed to the sophisticated energy-consuming system at the droplet-petal interface—the ingenious combination of a sticky superhydrophobic texture and an irregular texture. The pinning effect significantly modified the droplets' dynamic wettability. The sticky superhydrophobic surface is a type of superhydrophobic surface with various defects; thus, the above combination effect should be avoided when designing water-repellent surfaces. As we mentioned, the roses may reveal more "hydrophilic" at heavier precipitation. These findings may offer possibilities for designing high-efficiency energy conversion and harvesting[9,10,27].

Conflicts of interest

There are no conflicts of interest to declare.

Acknowledgments

This study was supported by the National Key Research and Development Program of China (Grant No. 2018YFA0703300), the National Natural Science Foundation of China (Grant No. 51575227, 51875243, 51706084), the Science and Technology Development Program of Jilin Province (Grant No. 172411GG010040701) and the Ph.D. Interdisciplinary Research Funding Scheme of Jilin University (Grant No. 10183201828).

Author contributions

C.Z. and Y.Z. conceived the study. Y.Z. and J.W. performed the experiments. J.Y., C.S. and Y.L. performed the simulations. Y.Z. wrote the paper. All the authors analyzed the data, proofread the paper, made comments.

References

[1] M. Nosonovsky, B. Bhushan, Energy transitions in superhydrophobicity: Low adhesion, easy flow and bouncing, J. Phys. Condens. Matter. (2008). doi:10.1088/0953-8984/20/39/395005.

[2] W. Barthlott, C. Neinhuis, Purity of the sacred lotus, or escape from contamination in biological surfaces, Planta. 202 (1997) 1–8.

[3] L. Chen, Z. Xiao, P.C.H. Chan, Y.K. Lee, Z. Li, A comparative study of droplet impact dynamics on a dual-scaled superhydrophobic surface and lotus leaf, Appl. Surf. Sci. 257 (2011) 8857–8863. doi:10.1016/j.apsusc.2011.04.094.

[4] P.-G. de Gennes, F. Brochard-Wyart, D. Quéré, Capillarity and Wetting Phenomena, 2004. doi:10.1007/978-0-387-21656-0.

[5] E. Bormashenko, T. Stein, R. Pogreb, D. Aurbach, "Petal effect" on surfaces based on lycopodium: High-stick surfaces demonstrating high apparent contact angles, J. Phys. Chem. C. (2009). doi:10.1021/jp900594k.

[6] L. Feng, Y. Zhang, J. Xi, Y. Zhu, N. Wang, F. Xia, L. Jiang, Petal effect: A superhydrophobic state with high adhesive force, Langmuir. (2008). doi:10.1021/la703821h.

[7] J.C. Bird, R. Dhiman, H.M. Kwon, K.K. Varanasi, Reducing the contact time of a bouncing drop, Nature. 503 (2013) 385–388. doi:10.1038/nature12740.

[8] J. Li, Z. Jing, F. Zha, Y. Yang, Q. Wang, Z. Lei, Facile spray-coating process for the fabrication of tunable adhesive superhydrophobic surfaces with heterogeneous chemical compositions used for selective transportation of microdroplets with different volumes, ACS Appl. Mater. Interfaces. (2014). doi:10.1021/am5015937.

[9] S. Zhang, J. Huang, Z. Chen, S. Yang, Y. Lai, Liquid mobility on superwettable surfaces for applications in energy and the environment, J. Mater. Chem. A. (2019). doi:10.1039/c8ta09403a.

[10] H. Li, W. Fang, Y. Li, Q. Yang, M. Li, Q. Li, X.-Q. Feng, Y. Song, Spontaneous droplets gyrating via asymmetric self-splitting on heterogeneous surfaces, Nat. Commun. (n.d.) 1–6. doi:10.1038/s41467-019-08919-2.

[11] A.B.D. Cassie, S. Baxter, Wettability of porous surfaces, Trans. Faraday Soc. (1944). doi:10.1039/tf9444000546.

[12] R.N. Wenzel, Resistance of solid surfaces to wetting by water, Ind. Eng. Chem. (1936). doi:10.1021/ie50320a024.

[13] D. Khojasteh, M. Kazerooni, S. Salarian, R. Kamali, Droplet impact on superhydrophobic surfaces: A review of recent developments, J. Ind. Eng. Chem. 42 (2016) 1–14. doi:10.1016/j.jiec.2016.07.027.

[14] C. Neinhuis, W. Barthlott, Characterization and distribution of water-repellent, self-cleaning plant surfaces, Ann. Bot. 79 (1997) 667–677. doi:10.1006/anbo.1997.0400.

[15] J. Lin, Y. Cai, X. Wang, B. Ding, J. Yu, M. Wang, Fabrication of biomimetic superhydrophobic surfaces inspired by lotus leaf and silver ragwort leaf., Nanoscale. 3 (2011) 1258–1262.

[16] T. Verho, C. Bower, P. Andrew, S. Franssila, O. Ikkala, R. RH, Mechanically durable superhydrophobic surfaces., Adv. Mater. 23 (2011) 673–678.

[17] L. Jiang, Y. Zhao, J. Zhai, A lotus-leaf-like superhydrophobic surface: a porous microsphere/nanofiber composite film prepared by electrohydrodynamics., Angew Chem Int Ed

Engl. 43 (2004) 4338–4341.

[18] X.M. Li, D. Reinhoudt, M. Crego-Calama, What do we need for a superhydrophobic surface? A review on the recent progress in the preparation of superhydrophobic surfaces, Cheminform. 36 (2007) 1350–1368.

[19] Q. Sun, H. Liu, T. Chen, Y. Wei, Z. Wei, Facile fabrication of iron-based superhydrophobic surfaces via electric corrosion without bath, Appl. Surf. Sci. 369 (2016) 277–287. doi:10.1016/j.apsusc.2016.02.069.

[20] M. Nosonovsky, B. Bhushan, Hierarchical roughness optimization for biomimetic superhydrophobic surfaces, Ultramicroscopy. 107 (2007) 969–979. doi:10.1016/j.ultramic.2007.04.011.

[21] H. Mertaniemi, R. Forchheimer, O. Ikkala, R.H.A. Ras, Rebounding droplet-droplet collisions on superhydrophobic surfaces: From the phenomenon to droplet logic, Adv. Mater. (2012). doi:10.1002/adma.201202980.

[22] L. Gao, T.J. McCarthy, How Wenzel and Cassie were wrong, Langmuir. 23 (2007) 3762–3765. doi:10.1021/la062634a.

[23] B. Bhushan, E.K. Her, Fabrication of superhydrophobic surfaces with high and low adhesion inspired from rose petal, Langmuir. (2010). doi:10.1021/la904585j.

[24] H. Teisala, M. Tuominen, J. Kuusipalo, Adhesion mechanism of water droplets on hierarchically rough superhydrophobic rose petal surface, J. Nanomater. (2011). doi:10.1155/2011/818707.

[25] S. Yang, J. Du, M. Cao, X. Yao, J. Ju, X. Jin, B. Su, K. Liu, L. Jiang, Direct insight into the three-dimensional internal morphology of solid-liquid-vapor interfaces at microscale, Angew. Chemie - Int. Ed. (2015). doi:10.1002/anie.201411023.

[26] H. Jin, Y. Li, P. Zhang, S. Nie, N. Gao, The investigation of the wetting behavior on the red rose petal, Appl. Phys. Lett. 108 (2016). doi:10.1063/1.4947057.

[27] A.L.L. Yarin, DROP IMPACT DYNAMICS: Splashing, Spreading, Receding, Bouncing…, Annu. Rev. Fluid Mech. 38 (2006) 159–192. doi:10.1146/annurev.fluid.38.050304.092144.

[28] Z. Che, O.K. Matar, Impact of Droplets on Liquid Films in the Presence of Surfactant, Langmuir. 33 (2017) 12140–12148. doi:10.1021/acs.langmuir.7b01901.

[29] C. Shen, C. Zhang, M. Gao, X. Li, Y. Liu, L. Ren, A.S. Moita, Investigation of effects of receding contact angle and energy conversion on numerical prediction of receding of the droplet impact onto hydrophilic and superhydrophilic surfaces, Int. J. Heat Fluid Flow. (2018). doi:10.1016/j.ijheatfluidflow.2018.09.015.

[30] R. Kannan, D. Sivakumar, Drop impact process on a hydrophobic grooved surface, Colloids Surfaces A Physicochem. Eng. Asp. (2008). doi:10.1016/j.colsurfa.2007.12.005.

[31] Y. Liu, L. Moevius, X. Xu, T. Qian, J.M. Yeomans, Z. Wang, Pancake bouncing on superhydrophobic surfaces, Nat. Phys. 10 (2014) 515–519. doi:10.1038/nphys2980.

[32] C. Zhang, Z. Wu, X. Zhang, Y. Yue, J. Wang, Effect of Feather Elasticity of Kingfisher Wing on Droplet Impact Dynamics, J. Bionic Eng. (2018). doi:10.1007/s42235-018-0061-5.

[33] C. Zhang, Y. Zheng, Z. Wu, J. Wang, C. Shen, Y. Liu, L. Ren, Non-wet kingfisher flying in the rain: The water-repellent mechanism of elastic feathers, J. Colloid Interface Sci. 541 (2019) 56–64. doi:10.1016/j.jcis.2019.01.070.

[34] P.B. Weisensee, J. Ma, Y.H. Shin, J. Tian, Y. Chang, W.P. King, N. Miljkovic, Droplet impact on vibrating superhydrophobic surfaces, Phys. Rev. Fluids. 2 (2017) 103601. doi:10.1103/PhysRevFluids.2.103601.

[35] Z. Li, Q. Kong, X. Ma, D. Zang, X. Guan, X. Ren, Dynamic effects and adhesion of water droplet impact on hydrophobic surfaces: bouncing or sticking, Nanoscale. 9 (2017) 8249–8255. doi:10.1039/C7NR02906C.

[36] Y. Shen, J. Tao, Z. Chen, C. Zhu, G. Wang, H. Chen, S. Liu, Rational Design of the Nanostructure Features on Superhydrophobic Surfaces for Enhanced Dynamic Water Repellency, ACS Sustain. Chem. Eng. 6 (2018) 9958–9965. doi:10.1021/acssuschemeng.8b01200.

[37] J. Li, Z. Jing, Y. Yang, L. Yan, F. Zha, Z. Lei, A facile solution immersion process for the fabrication of superhydrophobic ZnO surfaces with tunable water adhesion, Mater. Lett. 108 (2013) 267–269. doi:10.1016/j.matlet.2013.07.024.

[38] L. Moevius, Y. Liu, Z. Wang, J.M. Yeomans, Pancake bouncing: Simulations and theory and experimental verification, Langmuir. 30 (2014) 13021–13032. doi:10.1021/la5033916.

[39] C.M. Pooley, K. Furtado, Eliminating spurious velocities in the free-energy lattice Boltzmann

method, Phys. Rev. E - Stat. Nonlinear, Soft Matter Phys. (2008). doi:10.1103/PhysRevE.77.046702.

[40] B. Bhushan, M. Nosonovsky, The rose petal effect and the modes of superhydrophobicity, Philos. Trans. R. Soc. A Math. Phys. Eng. Sci. (2010). doi:10.1098/rsta.2010.0203.

[41] P.B. Weisensee, J. Tian, N. Miljkovic, W.P. King, Water droplet impact on elastic superhydrophobic surfaces, Sci. Rep. 6 (2016) 1–9. doi:10.1038/srep30328.

[42] R. Gupta, V. Vaikuntanathan, D. Sivakumar, Superhydrophobic qualities of an aluminum surface coated with hydrophobic solution NeverWet, Colloids Surfaces A Physicochem. Eng. Asp. 500 (2016) 45–53. doi:10.1016/j.colsurfa.2016.04.017.

[43] U.U. Ghosh, S. Nair, A. Das, R. Mukherjee, S. DasGupta, Replicating and resolving wetting and adhesion characteristics of a Rose petal, Colloids Surfaces A Physicochem. Eng. Asp. 561 (2019) 9–17. doi:10.1016/j.colsurfa.2018.10.028.

[44] B.A. Malouin, N.A. Koratkar, A.H. Hirsa, Z. Wang, Directed rebounding of droplets by microscale surface roughness gradients, Appl. Phys. Lett. 96 (2010) 94–97. doi:10.1063/1.3442500.

[45] T. Deng, K.K. Varanasi, M. Hsu, N. Bhate, C. Keimel, J. Stein, M. Blohm, Nonwetting of impinging droplets on textured surfaces, Appl. Phys. Lett. 94 (2009) 2–5. doi:10.1063/1.3110054.

[46] A. Alizadeh, V. Bahadur, W. Shang, Y. Zhu, D. Buckley, A. Dhinojwala, M. Sohal, Influence of substrate elasticity on droplet impact dynamics, Langmuir. 29 (2013) 4520–4524. doi:10.1021/la304767t.

[47] M.I. Smith, V. Bertola, Effect of polymer additives on the wetting of impacting droplets, Phys. Rev. Lett. (2010). doi:10.1103/PhysRevLett.104.154502.

[48] D. Zang, X. Wang, X. Geng, Y. Zhang, Y. Chen, Impact dynamics of droplets with silica nanoparticles and polymer additives, Soft Matter. (2013). doi:10.1039/c2sm26759d.

[49] C. Clanet, C. Béguin, D. Richard, D. Quéré, Maximal deformation of an impacting drop, J. Fluid Mech. 517 (2004) 199–208. doi:10.1017/S0022112004000904.

[50] P.D. Welch, The Use of Fast Fourier Transform for the Estimation of Power Spectra: A Method

Based on Time Averaging Over Short, Modified Periodograms, IEEE Trans. Audio Electroacoust. (1967). doi:10.1109/TAU.1967.1161901.

[51] S. Lin, B. Zhao, S. Zou, J. Guo, Z. Wei, L. Chen, Impact of viscous droplets on different wettable surfaces: Impact phenomena, the maximum spreading factor, spreading time and post-impact oscillation, J. Colloid Interface Sci. 516 (2018) 86–97. doi:10.1016/j.jcis.2017.12.086.

[52] L. Chen, Y. Wang, X. Peng, Q. Zhu, K. Zhang, Impact Dynamics of Aqueous Polymer Droplets on Superhydrophobic Surfaces, Macromolecules. 51 (2018) 7817–7827. doi:10.1021/acs.macromol.8b01589.

Robust adhesion of droplets via heterogeneous dynamic petal effects

Yihua Zheng[a], Chengchun Zhang [a, b*], Jing Wang [c], Yan Liu[a], Chun Shen [b], Junfeng Yang [d]

[a]Key Laboratory of Bionic Engineering (Ministry of Education), Jilin University, Changchun 130022, China

[b]State Key Laboratory of Automotive Simulation and Control, Jilin University, Changchun,130022, China

[c]College of Physics, Jilin University, Changchun 130012, China

[d]School of Mechanical Engineering, University of Leeds, LS2 9JT, United Kingdom

Abstract

Hypothesis

Bionics and dynamic interface wetting intensely appeal to many research communities due to their unique practical implications. The rose petals had a highly robust dynamic water-retaining capacity under heavy precipitation. We predicted that the roses became more "hydrophilic" at higher Weber numbers.

Experiments

Fresh rose petals were directly impacted by droplets, and facile artificial petal-like substrates and superhydrophobic substrates were used in the comparative analysis. The wetting dynamics of the droplet (e.g., topography, bounce dynamics, contact time, three-phase contact lines, and oscillations) were investigated when interacting with four selected target substrates.

Findings

The present work first time investigated the dynamic wetting rule of the sticky superhydrophobic substrates (SSHS). Simulated and experimental investigations confirmed that the unique coupling synergy between the pinning effect and the inhomogeneous micropapillaes resulted in lopsided contact line velocities, which remarkably suppressed the lateral oscillation and rebounding. This may be a new strategy when designing dynamic water-repellent surfaces and open a promising avenue for emerging areas such as super-efficiency energy conversion and harvesting.

Keywords: dynamic petal effect, droplet impact, asymmetric wetting, sticky superhydrophobic

1. Introduction

Rain droplets on lotus leaves may be less striking than rain droplets on rose petals. Water droplets can attach to rose petals without rolling off, even at great tilt angles. However, water droplets cannot remain on lotus leaves after a rain. The “lotus effect” is synonymous with superhydrophobicity, and a superhydrophobic surface(SHS) exhibits a static apparent contact angle (CA, θ) of greater than 150° with a very low contact angle hysteresis (CAH, θ_{CAH})[1–4]. Interestingly, rose petals can exhibit an extremely high CA similar to that of the “lotus effect”, but with high CAH (Fig. 1a)[5]. This "sticky superhydrophobic” substrate (SSHS) phenomenon known as the "petal effect" was first proposed by Jiang et al.[6] and has since drawn much research attention due to its widespread use in emerging fields such as self-cleaning[7], droplet transfer, transportation[8], biochemical separation, and energy harvesting[9,10]. In addition, studying the dynamic wetting mechanism of an SSHS provides information for enhancing functional surface designs.

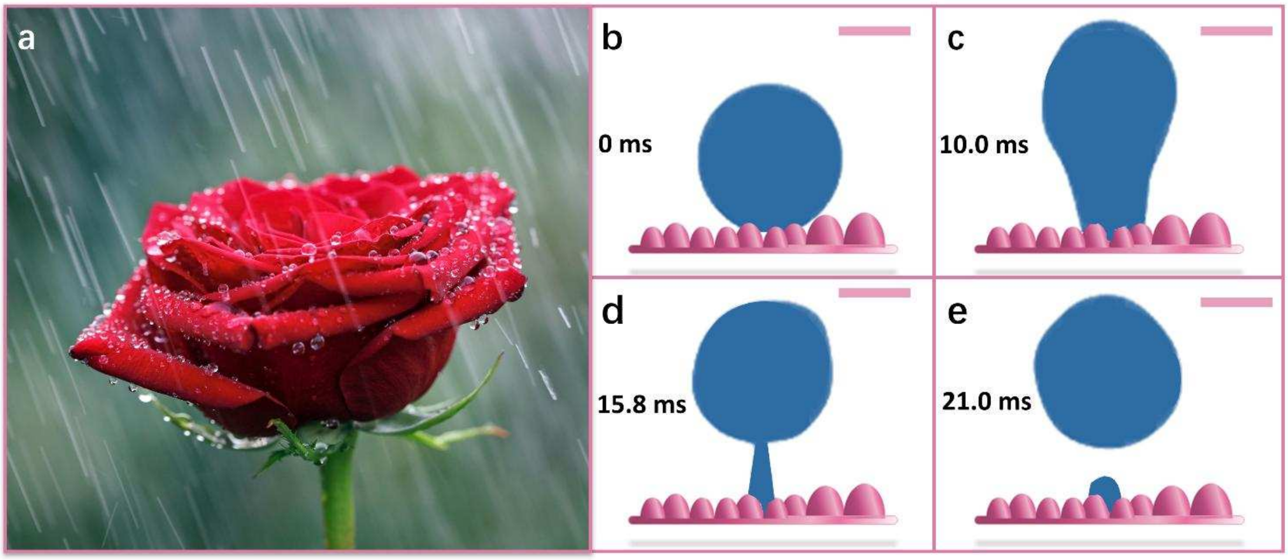

Fig. 1 Dynamic wetting phenomenon on rose petals. **(a)** Retention of spherelike droplets on rose petals in the rain. **(b-e)** Schematic diagram of the interfacial process of a droplet impacting a rose petal at low-impact velocities. The scale bar=1 mm.

Generally, the static-wetting state of rough surfaces can be explained by the classical wetting theory of Cassie-Baxter[11] and Wenzel[12]. In the Cassie-Baxter model, the rough solid surface is completely filled with liquid, resulting in high water adhesion. However, entrapped air is observed in the Wenzel model, which is attributed to hydrophobicity[13]. The superhydrophobicity exhibited on the lotus leaf results from the combination of convex epidermal cells and extremely low-density biowax layers[14]. The lotus effect should be governed by the idealized Cassie-Baxter model. For the lotus effect, research on fabricating and characterizing biomimetic surfaces is trending, both theoretically and experimentally[15–21]. In contrast, few in-depth studies have examined the petal effect; thus, the accurate mechanism of the petal effect wetting behavior remains unclear[22]. Nonetheless, the Cassie-Baxter and Wenzel models are used by most scientists to explain wettability at the interface. Adhesion of water droplets to rose petals has been attributed to the Wenzel state based on the geometric parameters of the rose petal surface determined for both biological and artificial samples. These parameters include the diameter, spacing and secondary nanostructure of the micropapillae[23](Fig. 1 b-e). In contrast, the opposite conclusion has also been suggested, in that the petal's microstructure is considered to benefit adhesion, but this conclusion cannot be explained by the classic Cassie-Baxter wetting theory[24]. Thus, the rose petal wetting mechanism seems puzzling. S. Yang et al.[25] observed that the interaction between droplets and rose petals was completely in accordance with the Wenzel state, and these authors found no air cushion using micro computed tomography. Visualization technology has been developed, which has facilitated analyzing this mechanism. Optical microscopy observations using micron-scale resolution have recently shown that the wetting behavior of droplets on rose petals is unstable because gas moves slowly from the space over the liquid, thus altering the wetting state. This is a mutual transformation from the Cassie and Wenzel states[26]. This contradictory conclusion was likely reached because dynamic observations were applied to the latter; that is, the movable air cushion disappeared after connecting to the atmosphere, resulting in continuous wetting at the three-phase contact line (TCL).

Thus, the static-wetting mechanism of the petal effect remains unclear, and determining its precise dynamic wetting process is challenging. Experiments and simulations in which droplets impact the substrate have long been used to investigate the dynamic wettability of natural, artificial and chemically heterogeneous surfaces[27]. To our knowledge, previous investigations of the substrate's configuration after being impacted by the droplet mainly included liquid film[28], superhydrophilicity[29], hydrophobicity[30], superhydrophobicity[31], elastic superhydrophobicity[32,33], and vibrating superhydrophobicity[34]; however, no reports regarding droplet impact on SSH surfaces (the petal effect) have been published. Li et al.[35] reported the dynamic wetting characteristics of water droplets on various substrate configurations at CA = 160°, 154°, 153°, 122°, 124°, and 119°. Shen et al.[36] verified that a relationship exists between the trapped air and the interface adhesion when a droplet impacts a sticky hydrophobic substrate. In the two aforementioned studies, the droplets were released from the same height as that impacting the substrate, which was insufficient to summarize the rules of dynamic wetting on sticky superhydrophobic surfaces.

This paper describes the dynamic wetting rule on a SSHS (i.e., the petal effect) by comparing the wetting state on a superhydrophobic surface. The quantitative (experiments) and qualitative (simulations) investigation confirm that the dynamic unbalance wetting mechanism of the petal effect is due to the coupling of the lateral interaction of the droplets with the pinning effect, thus providing novel insights into why rose petals can retain water droplets and new rational guidelines for wetting functional surface design.

2. Experimental materials and methods

2.1 Surface fabrication and characterization

To capture the commonality of droplet dynamics on the SSHS, three target substrates were fabricated, including the rose petal surface (RPS) and engineering sticky superhydrophobic surfaces (SSHS-1 and SSHS-2). Besides, the superhydrophobic surface (SHS) is used for comparative verification.

2.1.1 Rose petal surface (RPS)

A fresh red rose was purchased from a flower market (Changchun, China), and a piece of the rose petal (15 mm × 1.5 mm) was fixed to a glass sheet which was neither cleaned nor altered.

2.1.2 Sticky superhydrophobic surface (SSHS)

We replicated the surface (SSHS-1) invented by Chen et al.[37], with some modifications to the chemical reactions. One-millimeter-thick zinc foil was ultrasonically cleaned in acetone and deionized water. The zinc foil was etched in hydrochloric acid for 15 seconds, then washed thoroughly in deionized water. Next, the zinc foil was etched in hydrochloric acid for 15 s, then immersed in 0.01 mol/L $CuSO_4 \cdot H_2O$ for 12 minutes, thoroughly washed again in deionized water, and immersed in 0.005 mol/L $CH_3(CH_2)_{16}COOH$ for 30 minutes. We also established a micron-scale with arrays on paraffin with low surface energies (SSHS-2) for comparison. (S1.2, Supplementary Information).

2.1.3 Superhydrophobic surface (SHS)

The 2-mm-thick square copper plate was etched in hydrochloric and sanding with sandpaper then treated with 1H,1H,2H,2H-perfluorodecyl trichlorosilane (Aladdin, Inc., China) via chemical vapour deposition.

2.1.4 Surface characterization

All characterization tests were performed indoors at 25℃. The surface morphology was characterized by scanning electron microscopy (SEM; EVO MA 25/LS, ZEISS, Inc., Germany) with 20-kV accelerating voltage and a three-position ultra-depth microscope (Smartzoom 5, ZEISS, Inc., Germany). The apparent contact angles were measured using a contact angle meter (DSA 22 KRUSS, Germany), wherein the water droplet volume was 4 μL.

2.1.5 Experimental apparatus and image analysis

To analyze the dynamic wetting behavior of the droplets, an experimental system was established to observe and record the droplet impacting the substrate (Fig. S1 in Supplementary Information). This system generates the water droplets (2.14±0.01 mm) using a 0.24-mm metal needle and a syringe driven by a microstepping motor. Using another microstepper motor, the droplet-to-substrate distance (H) can be varied, resulting in speeds of v=0.308–1.128 m/s. The resulting corresponding dimensionless numbers are the Weber number $W_e=\rho v^2 D_0/\gamma$= 4–50, capillary number $C_a=\mu v/\gamma$= $(4–16)\times10^{-3}$, Reynolds number $R_e=\rho v D_0/\mu$= 866–3120, and Ohnesorge number $O_h=\mu/(\rho\gamma D_0)^{1/2}$= 2×10^{-3}, with a density of ρ=997 $Kg\cdot m^{-3}$, surface tension of $\gamma=72\times10^{-3}$ N/m, and dynamic viscosity of $\mu=0.89\times10^{-3}$ Pa·s, which are the water's physical parameters.

2.1.6 Simulations

Qualitative simulation analysis was performed via the lattice Boltzmann method(the D3Q9 grid) [38,39].

3. Results and discussion

3.1 Morphology and wettability of the target substrates

Fig. 2 illustrates the morphology and adhesive states of the selected substrates (RPS, SSHS-1, SSHS-2 and SHS). The RPS could be visually characterized by a three-position ultra-depth microscope at 1000× magnification (Fig. 2a). The irregular array consisted of micropapillaes averaging 9±2 μm high and 19±2 μm in diameter (similar to previous studies[6,40]), which were semiautomatically obtained from the written code in MATLAB and the open-source software ImageJ by analyzing the selected images. The inset plots in Fig. 2a illustrate that the CA of the RPS was 154° ±2°, and a 4-μL droplet could adhere to the surface with a tilt angle of 180°. Similar wetting states also occur on sticky superhydrophobic zinc foils fabricated by chemical etching. The insets in Fig. 2c show that the CA of the SSHS-1 is 157°±2°, and it exhibited high adhesion. Fig. 2d shows the SHS with CA=153°±2° and θ_{CAH}=3°±1°, indicating a typical lotus effect phenomenon, which is consistent with previous studies[41,42].The microstructures in Fig. 2e–g are SSHS-2, which are manufactured by rapidly peeling off the copper mesh that was tightly attached to the solidified paraffin and the colored box indicates the corresponding selected area. The inset plot in Fig. 2e likewise shows a similar petal effect phenomenon, indicating CA=156°±2° with a large adhesive force. We established a diagrammatic sketch of a typical SSHS-2 microstructure (Fig. 2h), in which the corresponding statistical geometric parameters of the typical microstructures were short-side length: a=85±2 μm, long-side length: b=220±2 μm, width: w=50±2 μm, and height: h=50±2 μm.

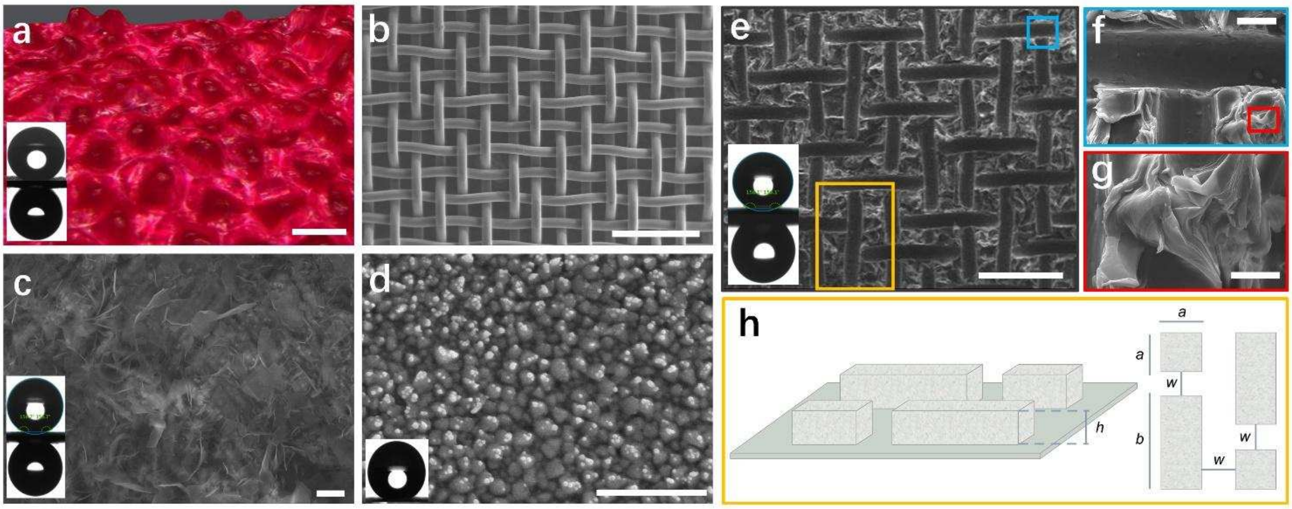

Fig. 2 Characterization of the static wettabilities of (a) RPS, (b) 200-mesh copper mesh, (c) SSHS-1, (d) SHS and (e–h) SSHS-2. **(a)** Image of a fresh rose petal captured by a 3D super depth-of-field microscope at 1000× magnification (scale bar=25 μm). The darker red indicates the top of the mastoid, while the relatively low area is shown in light red. The RPS exhibited a petal effect phenomenon with CA=154°±2° and high adhesion, as illustrated in the insets. **(b)** SEM image of the 200-mesh copper mesh (scale bar=500 μm). **(c)** SEM image of SSHS-1 (scale bar=4 μm). The insets indicate that the CA=156°±2° with the high adhesive phenomenon. **(d)** SEM image of a superhydrophobic surface with CA=153°±2° (see inset). The scale bar=500 nm. **(e)** Regular array of paraffin cubes with the same spacing and height. The insets indicate that CA=157°±2° with markedly high adhesive behavior (scale bar=300 μm). **(f)** T-shaped paraffin microstructure (blue boxes). Compared with the top of the raised paraffin square column, the trace of the single copper wire was almost smooth at the same magnification factor. (scale bar=40 μm) **(g)** The top of the raised paraffin square column is shown in red boxes. **(h)** Schematic diagram of a typical microstructure model (orange boxes). The microstructure dimensional parameters were a=85±2 μm, b=220±2 μm, w=50±2 μm, and h=50±2 μm (scale bar =20 μm).

3.2 Qualitative and quantitative analysis of Non-uniform lateral interaction on the SSHS

Simulations are performed to qualitatively explain the effect of the unbalanced Young's force dF_t on the wettability of the interface. The micropapillaes and droplets are of the same order of magnitude to facilitate intuitive analysis (Fig. 3a).Two-phase fluid dynamics equations are solved using the D3Q19 grid based on a lattice Boltzmann algorithm[38,39]. The micropapillaes of the RPS are arranged in regular arrays during a simulation. In addition, the larger micropapillaes (height =0.4 mm with diameter =0.4 mm) are configured with a CA of 150° to counteract the superhydrophobicity, whereas the CA of the secondary micropapillaes (height =0.2 mm with diameter =0.2 mm) is configured for 110°. The high-impact velocity droplets oscillated randomly and finally adhered to the rose petals; otherwise, the droplets have bounced at a low-impact speed. The droplets tend to adhere to the petals with the increasing Weber numbers, as reflected in the residual droplets (red dotted circle in Fig. 3e). The additional viscous dissipation during the droplet-petal interaction in the high Weber number state is attributed to cooperation between the irregular morphology[43] (micropapillaes, Fig. 2a) and the sticky superhydrophobicity of the rose petals. Anomalous droplet formation was initialized during the spreading phase; however, the asymmetrical speed of the moving contact line was evident in the receding phase from a two-dimensional perspective in the schematic (Fig. 3 a-d). The lateral rebounding of a droplet can be manipulated because of the uneven gradient on the textured surface[44] and the unbalanced Young's force expressed as

$$\mathrm{dF} = \sigma\left|\cos\theta_{\mathrm{Rt}} - \cos\theta_{\mathrm{Lt}}\right|\mathrm{ds}, \tag{1}$$

where $\cos\theta_{\mathrm{Rt}}$ and $\cos\theta_{\mathrm{Lt}}$ are the apparent contact angles of the right and left sides(Fig. 3 a-d), respectively, which were evaluated instantaneously by image analysis. $\mathrm{d_s}$ is the differential of the moving contact line, and dF is the transient unbalanced Young's force, which resists the inertia of the droplet. Thus, as $\left|\cos\theta_{\mathrm{Rt}} - \cos\theta_{\mathrm{Lt}}\right|$ increases (the droplet is more distorted), $\mathrm{F_t}$ also increases, resulting in a more "hydrophilic" substrate, which is consistent with that shown in Fig. 3e. Here, the effective unbalanced Young's force ($\mathrm{F_e}$) can be simplified as

$$\Delta \propto \left|\cos\theta_{\mathrm{Rt}} - \cos\theta_{\mathrm{Lt}}\right| \propto \frac{1}{5}(\lg\left|\theta_{\mathrm{Rt}} - \theta_{\mathrm{Lt}}\right|) \tag{2}$$

via analyzing the simulations. Δ contains a constant $\frac{1}{5}$, so that Δ is in the same order of magnitude as the quantitative result, which is advantageous for comparison verification.

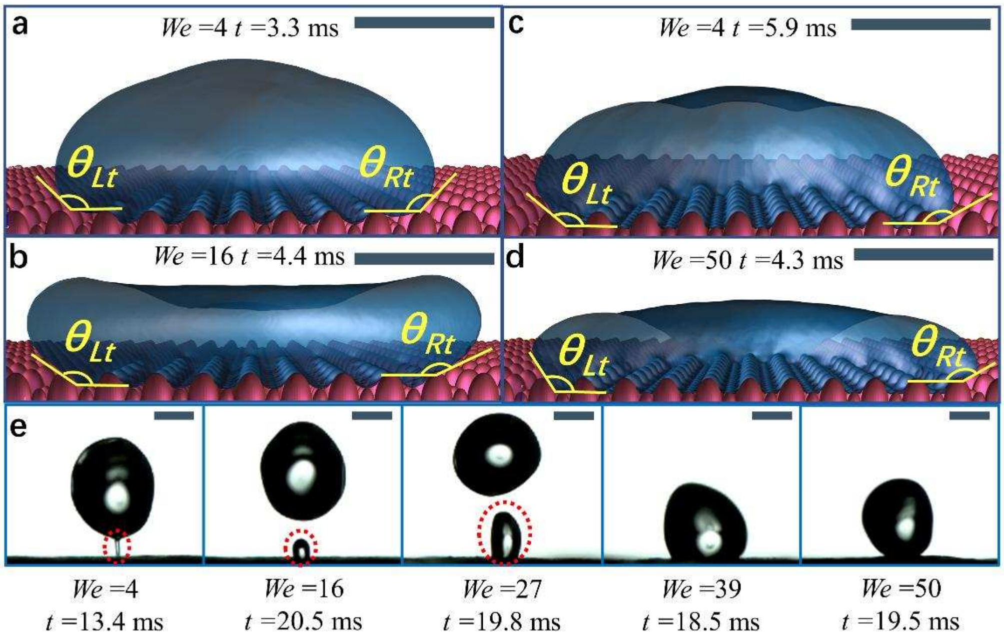

Fig. 3 Simulated and experimental analysis and verification of the unbalanced Young's force caused by the SSHS. **(a)-(d)** Simulation analysis of droplets are observed to be in the most laterally unbalanced. Unbalanced droplet morphology due to irregular micropapillaes in the receding phase. Consequently, the Young's force increases, causing additional energy dissipation. The results of the simulation show that the difference between $\cos\theta_{Lt}$ and $\cos\theta_{Rt}$ is more significant as the Weber number increases, so higher F_e eventually lead to droplets adhesion. The scale bar= 1.8 mm. **(e)** The quantitative similarity of various morphologies of pinging tiny droplets (red dotted circle) on a rose petal as the Weber number increased. The rose petals became more "hydrophilic". The scale bar= 1 mm.

However, the aforementioned effective unbalanced Young's force F_e is transient and difficult to quantify via experiments. Thus, the dimensionless size of the residual droplets, $\lambda = D_r / D_0$, is used to investigate the extent of the dynamic petal effect due to the intuitive result of the dynamic petal effect is reflected in the residual moisture on the RPS, as shown in Fig. 3e. These retained liquids on the RPS are essentially caused by varying degrees of the Cassie-to-Wenzel transition[11,12] which can be regarded as the partial wetting state. This partial wetting state is mainly governed by the effective water hammer pressure verified by Tao et al[45],

$$P_{EWH} = k\rho Cv, \quad (3)$$

where C is the speed of sound in water, and k is the fitting parameter of the corresponding experiment. Herein, $v \propto We^{0.5}$ and then $P_{EWH} \propto \alpha We^{0.5}$,where $\alpha = k\rho C$. In this case, we assumed that that dF_t is in a two-dimensional environment, thus dF_t and λ are in the same dimension and related. Together with Eq. (1-3), the quantitative estimation of dynamic petal effect of RPS would yield $dF_t \propto (\zeta = \alpha We^{\beta\lambda}) \propto \Delta \propto \alpha We^{\gamma}$ .Thereby,

$$\zeta = 0.0366(\frac{\rho v^2 D_0}{\gamma})^{0.633}, \quad (3)$$

where $4 < W_e = \frac{\rho v^2 D_0}{\gamma} < 27$ .Eq. (3) are satisfied in our experiments (Fig. 3e and Fig. 4a): the dynamic water-repellency of the SSHS is only closely related to the impact velocity of the droplets (v). The limit (W_e<4) was considered as the inconspicuous dynamic petal effect regime, while the critical total wetting state occurs when W_e>27. Furthermore, the simulation results (Fig. 3 a-d and Fig. 4b-d) qualitatively reveal the adhesion water caused by the lateral effect of the droplets of the SSHS in this study. Thus, the aforementioned effective unbalanced Young's force F_t would yield

$$\Delta = 0.0259(\frac{\rho v^2 D_0}{\gamma})^{0.638}. \quad (4)$$

Herein, $4 < W_e = \frac{\rho v^2 D_0}{\gamma} < 50$ .The results of the simulation (the blue line in Fig. 4a) satisfactorily confirm the positive effect of the lateral effect on droplet adhesion. The RPS—with its unique asymmetric natural sticky superhydrophobic, resulting in solid edges with discontinuous physical properties (e.g. wettability) that directly affect the receding speed of the three-phase contact line, which is striking at higher at high Weber numbers. As shown in yellow dotted circles in Fig. 4d, significant asymmetric receding line velocities and morphology are observed on both sides of the droplet, in contrast, symmetrical edge velocities occur at low Weber numbers(Fig. 4 b-c). Qualitatively, the synergy of the multiple lateral asymmetric effects and sticky will make the SSHS more sticky and "hydrophilic" at high droplet impinging velocities regime (see the insets in Fig. 4).

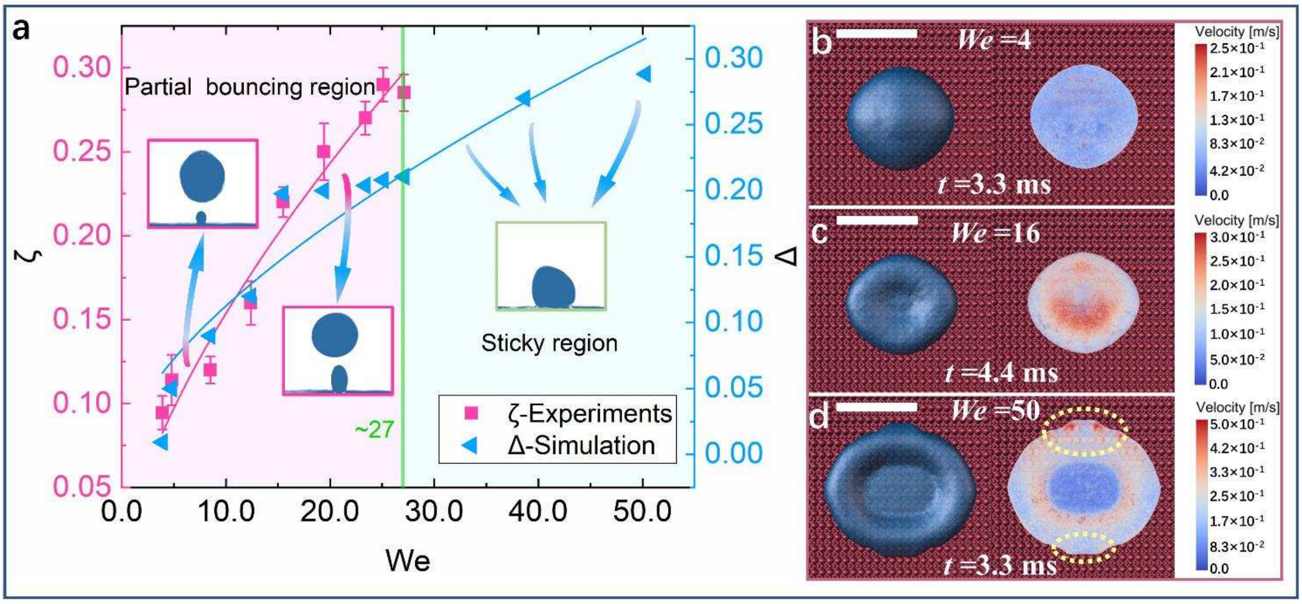

Fig. 4 Quantitative and qualitative comparisons of the effects of multiple lateral pinning on the RPS's wetting characteristics. **(a)** Investigations of the correlation between lateral effects and sticky adhesion on the SSHS. The insets show the extent of the dynamic petal effect, from pinning tiny droplets (partial rebound, lilac region) to no bouncing sticky region (light green area) as the Weber number increases. Satisfactory qualitative similarities are revealed in experimental and numerical results (purple and blue fitted line)**.** The critical of the partial bouncing region and sticky region is W_e = 27 (green line). **(b)-(d)** The simulated velocity field as the droplets develop to their most asymmetrical morphology. Axisymmetric droplet morphology occurs under the low Weber number regime (W_e = 4), but note that the higher impinging velocities (corresponding to W_e = 50) result in remarkable unbalanced receding velocities (yellow dotted circle).Both versions of the investigation confirmed the same characteristic that asymmetric interactions caused by high weber number reduce the possibility of droplet bouncing. The scale bar=4 mm.

3.3 Droplet bounce dynamics

In order to verify the above-mentioned theory, three SSHSs (the RPS, SSHS-1 and SSHS-2) and a SHS were selected as the target substrates. When a droplet hits a rough solid surface, it may bounce or stick, after undergoing the spreading and receding stages. The interfacial behavior of the droplets corresponds to the hydrophobicity (e.g., CA and CAH) of the substrate and is significantly affected by the wettability (e.g., high adhesion) of the interface[27]. We examined the droplet impact on the four aforementioned surfaces. For droplets, the low-impact velocity resulted in a low kinetic energy level. Fig. 5 illustrates the dynamic wetting process of the droplets on RPS, SSHS-1, SSHS-2 and SHS at a very low Weber number (W_e= 4, corresponding to v=0.362±0.001 m/s; see also Supplementary Movie S1). Droplets with sufficient kinetic energy can generally bounce off sticky superhydrophobic substrates at a very low Weber number, W_e= 4 (Fig. 5 a–c). Partial pinning occurred at the bottom of the droplet resulting in a slightly longer contact time than that on the SHS (see S3 in Supplementary Information for more details). The bounce of the drop was partially inhibited when the droplet impacted the sticky superhydrophobic substrate compared with that on the superhydrophobic substrate under the corresponding impacting velocity.

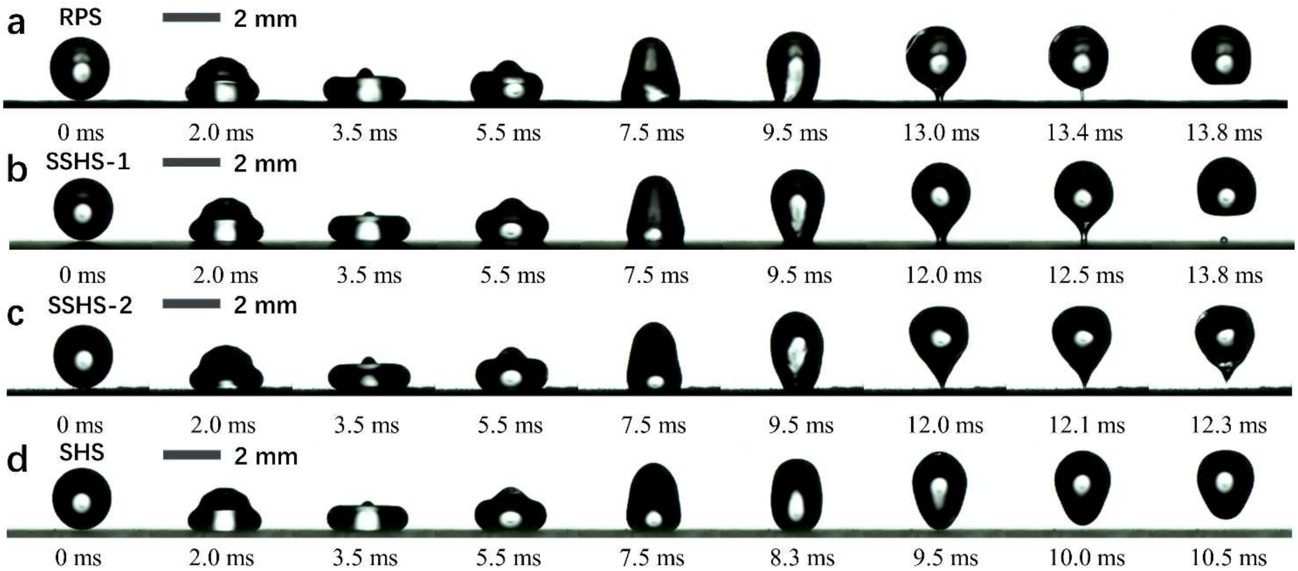

Fig. 5 Snapshots of the droplets' dynamic behavior on RPS, SSHS-1, SSHS-2 and SHS (W_e= 4, corresponding to v=0.362±0.001 m/s). **(a–c)** Time evolution of an impacting droplet on RPS, SSHS-1, SSHS-2, respectively. The droplet morphology becomes asymmetrical during the receding phase. Droplets can still rebound, but the substrates exhibit some viscosity. **(d)** Impact phase diagram of a droplet impacting the SHS. The droplet lifts off the substrate with less contact time and remains more symmetric compared with that on the aforementioned substrates. Supplementary Movie S1 provides more details. The scale bar=2 mm.

As the Weber number increases slightly (W_e= 16, corresponding to v=0.723±0.001 m/s), the SSHS plays a more vital role in the droplets' dynamic behavior than does the SSH. Detaching the droplet from the SSHS was more difficult and differed greatly from its interaction on the SHS (Fig. 6; Supplementary Movie S2). The droplet morphology on all target substrates was almost synchronous during the spreading phase (0 ms < t < 3.5 ms) and was independent of the target substrate's wettability and impact velocity, which is consistent with previous studies[33,36,46]. For the RPS, the geometric center of the droplet changed and gradually moved away from the axis of symmetry, indicating more sensitivity to the impact velocity of the droplet after 3.5 ms than at the We of 4 (Fig. 5 a and Fig. 6a). Thus, the droplet exhibited difficulty in rebounding completely, even with a higher initial kinetic energy, as illustrated by the residual secondary droplets on the sticky substrate (blue and green dotted circles in Fig. 6a, see also S4 in Supplementary Information). Interestingly, similar wetting phenomena were observed on both SSHS-1 and SSHS-2 (Fig. 6b–c). One droplet was difficult to lift off and was even pinned to the substrate (red dotted circle in Fig. 6c). Instead, the droplet lifted off from the SHS quickly after undergoing a spreading and retracting phase similar to that of the above corresponding testing condition. We confirmed that the dynamic response of the droplets is critical to wetting the SSHS interface during the receding phase when $4 \leq W_e \leq 16$.

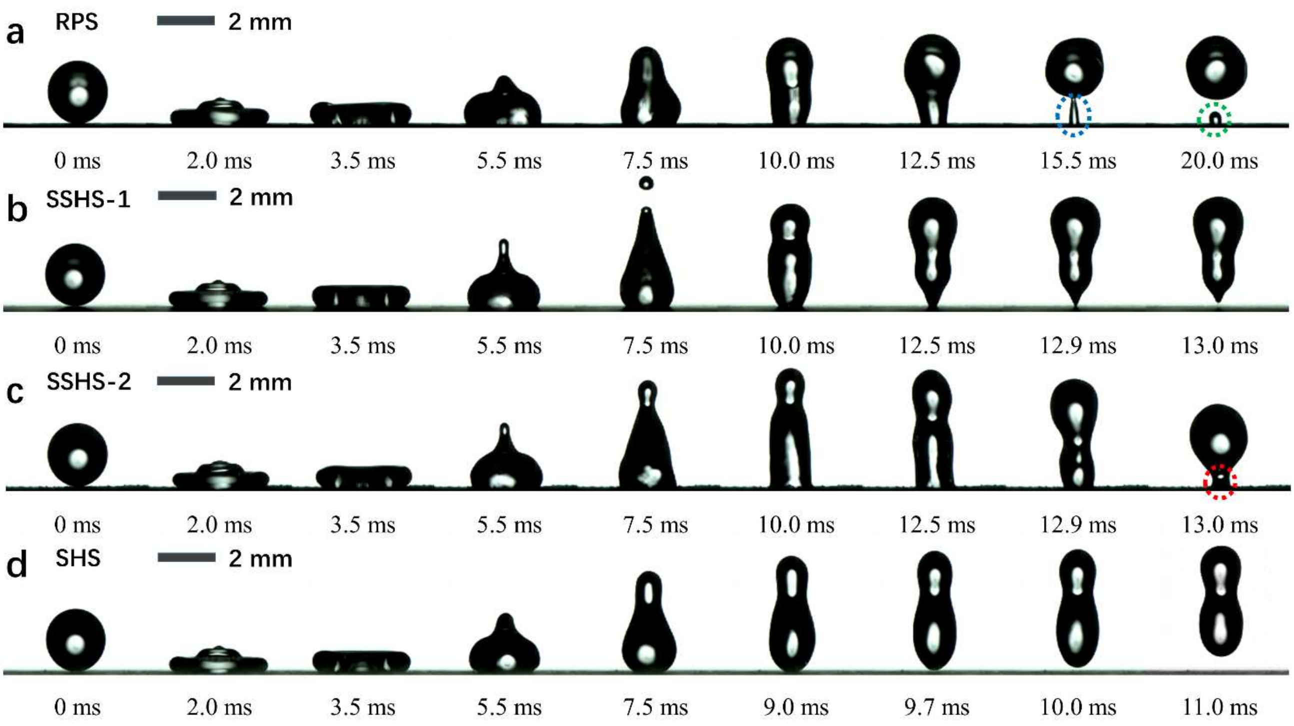

Fig. 6 Sequential snapshots of the droplets' dynamic behaviors on the RPS, SSHS-1, SSHS-2 and SHS (W_e=16, corresponding to v=0.723±0.001 m/s). **(a)** Impact phase diagram of a droplet impacting the RPS. Note that this droplet was observed to be extremely asymmetric at t=5.5 ms. During the

rebound phase, the liquid bridge (blue circle) is captured between the ejecting droplet and the substrate. A residual secondary droplet is shown in the green circle. **(b)** Drop impacting the SSHS-1 with a tiny droplet ejecting at t=7.5 ms. **(c)** A droplet is completely trapped on the SSHS-2. A larger liquid bridge is observed at the interface and is circled in red. **(d)** Sequential phase diagram of a droplet impacting the SHS. Almost no adhesion was observed (Supplementary Movie S2). The scale bar=4 mm.

Interestingly, as we predicted, the spreading phase of the droplets was also affected by the substrate configuration, such as in the receding phase when the impact velocity was high (W_e=50, corresponding to v=1.304±0.001 m/s), which appears to be inconsistent with previous studies. In the present study, the surface tension and viscosity of the water were constant and were factors that inhibited the droplet from receding[47]. Fig. 7 shows the dynamic process of the droplet impacting the RPS and SSHS-2 (Supplementary Movie S3). The droplet morphology is extremely asynchronized during the spreading phase after t=2 ms. In addition, the droplet showed a maximum twist compared with all previous test conditions and exhibited a surprisingly dF and could not to lift off the substrate (Fig. 7a). Previously, we confirmed that droplets are more likely to adhere at high Weber numbers, but did not qualitatively clarify the droplets' reciprocating oscillation on the RPS. Once the de-pinning effect is initialized (red box in Fig. 7a), the de-pinning force for the moment, including the inward and upward forces, will be activated (green box in Fig. 7a). The mechanism of the corresponding state can be qualitatively explained by the blue box in Fig. 7b and the green box in Fig. 7c, respectively. Note that dF, with both upward and inward vectors, drives the leftmost liquid to hit those adjacent portions with lower receding velocities, instead, the de-pinning does not occur on the rightmost, thus the droplet exhibits unbalanced and eventually cause reciprocating oscillation of a droplet on a rose petal. The free liquid-gas interface adjacent to the petal is pinned again, causing multiple viscous energy dissipation, and the petal eventually becomes more "hydrophilic".

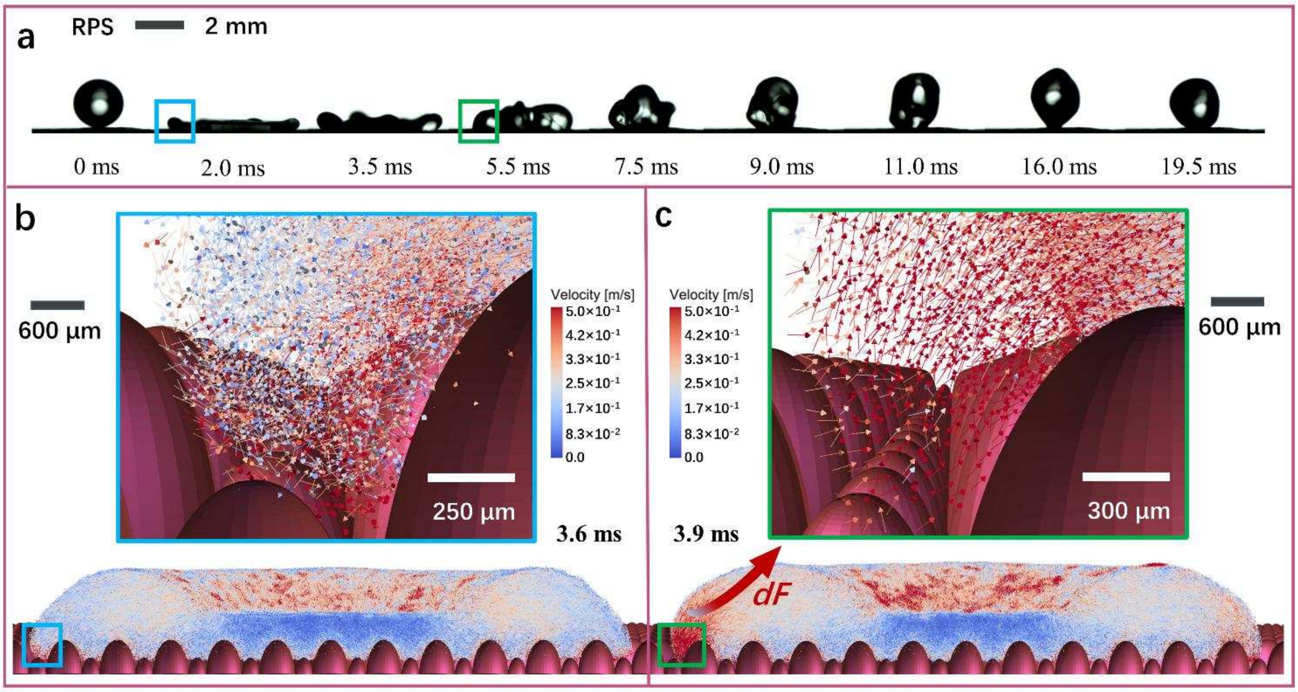

Fig. 7 Impact of droplets on the RPS at high velocities (W_e=50, corresponding to v=1.304±0.001 m/s). **(a)** A droplet impacts the RPS, exhibiting a sharp anisotropic vibration that prevents it from bouncing off the substrate. As we predicted, the non-negligible unbalanced Young's force increases with higher Weber number regime due to the strong asymmetrical solid-liquid interaction (See Supplementary Movie S3 for more details). The scale bar=2 mm. **(b)-(c)** Side-view snapshots of force analysis of the de-pinning procedure (3.6-3.9 ms). The velocity vectors of the particles are represented by arrows, and the zoomed area (blue box, the scale bar=250 μm) indicates that the high inward velocities vector only occurs at the wall before de-pinning. Subsequently, the leftmost particles have both inward and upward velocity vectors, which then impact adjacent low-velocity portions, causing unbalanced oscillations and additional energy dissipation, ultimately depleting the energy of the upward impact of the droplets(green box, the scale bar=300 μm).

3.4 Unique mechanism for suppressing oscillation

The TCL is always accompanied by the whole process of solid-liquid interaction, which does not merely increase the effective interfacial friction but also suppresses the bouncing droplets[48]. The size of the annular TCL can be quantified by the length of the horizontally overlapping lines (D_h). As a function of the time scale, D_h was normalized by the initial diameter D_0 (Fig. 8). A droplet can bounce from both a sticky superhydrophobic substrate and a superhydrophobic substrate, which was reflected in the similarity of the TCL when the droplet underwent a symmetrically evolved interaction with the substrate (W_e =4, Fig. 8 a). The TCL evolved as a function of time scales, and the peaks of these curves correspond to the droplet's maximum spreading diameter (D_{max}) when it impacted the four selected substrates. The maximum spreading factor β_{max}= $(D_{max}/D_0) \sim W_e^{0.25}$ =1.405 is a critical parameter for evaluating inertia-dominated wetting kinetics based on mass conservation, which is consistent with the conclusions drawn by Clanet et al.[49]. This also indicates that the droplet's dynamic response is independent of the substrate configuration and remains dominated by inertia within a low Weber number regimen. For the higher W_e=50, the effect of the substrate configuration on the impact dynamics of the droplets was more effective. All droplets accomplished the spreading process in 3 ms, then experienced a more time-consuming receding phase (Fig. 8b). The distinguishable curves indicate that the droplet morphology was more sensitive to the substrate configuration than that within the high Weber number regimen. We also noticed that the rose petals exhibited the strongest robust liquid viscous effect[48] compared with the other three target substrates during the solid-liquid interaction process. In addition, the comparative analysis indicated that the droplet spreading was strongly suppressed at the liquid-petal interface, and the excess restoring force (reflected in the viscosity of the droplets) was transformed into the surface energy of the irregular twisting droplet (t =7.5 ms in Fig. 7a). The irregular droplet twist caused the surface energy to be consumed by both the viscosity of the droplet and the partial pinning effect of the petals based on the energy conservation argument, eventually leading to droplet adhesion. Conversely, the spreading and retraction of the droplets were maximized because the SHS exhibited the lowest contact angle hysteresis among all selected substrates[2,3]. Analysis of the contact line showed that this twist was relatively stable, while the other three selected substrates exhibited larger fluctuations.

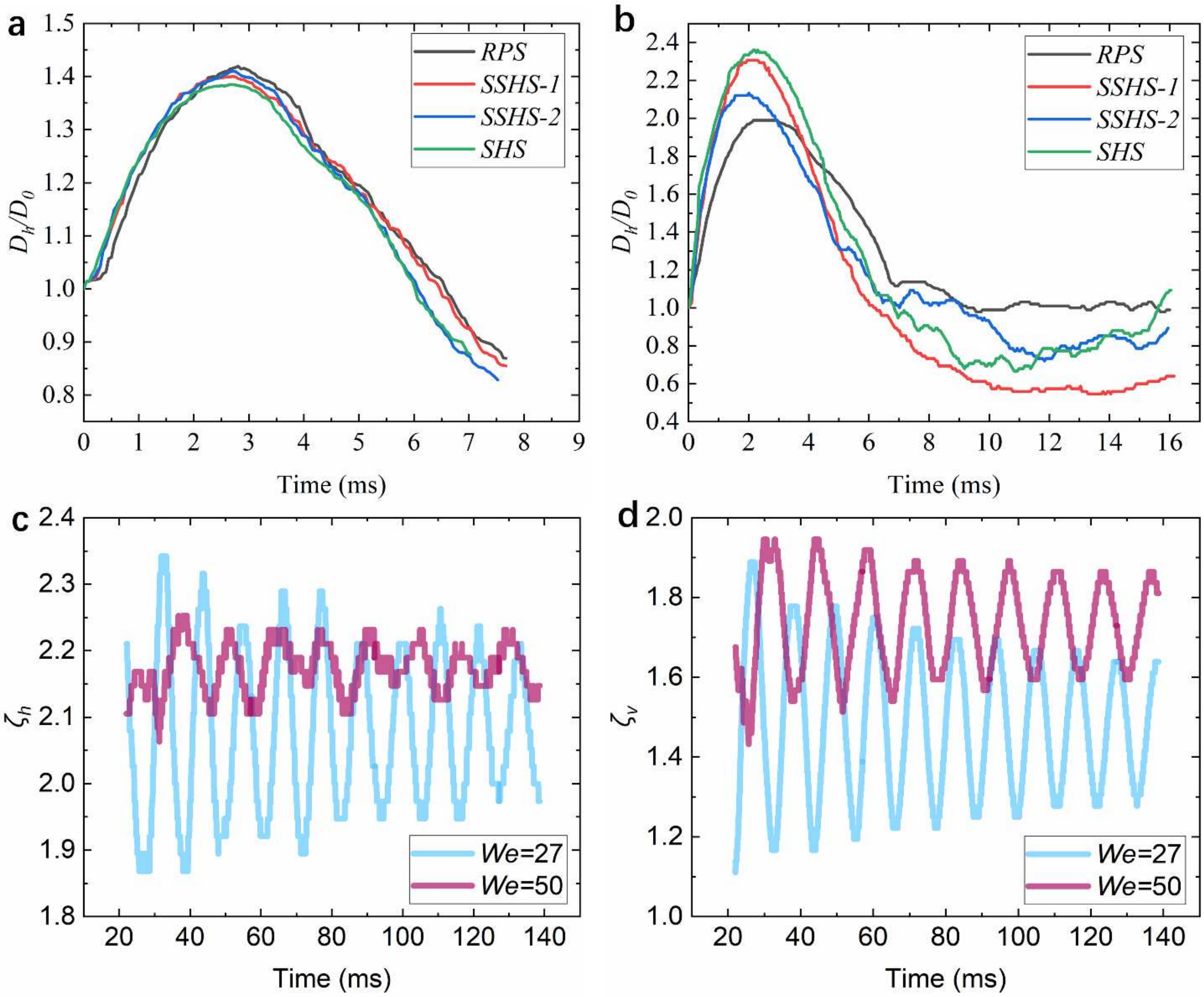

Fig. 8 Transient contact diameter of the droplet impacting the four substrates at **(a)** W_e=4 and **(b)** W_e=50. The difference was not significant under the low Weber number regimen. Nevertheless, the substrate configuration dominated the droplet topography at W_e=50. **(c)** Comparative analysis of the horizontal flatness factor, ζ_h, under moderate (W_e=27) and high (W_e=50) Weber numbers. The lateral droplet response was consistent in the latter case. **(d)** Comparative analysis of the vertical flatness factor, ζ_v, under moderate (W_e=27) and high (W_e=50) Weber numbers. Unexpectedly, the high-impact velocity of a droplet led to a lower amplitude.

Attenuation of the droplet oscillation is similar to the underdamped harmonic oscillator, which has the characteristics of a vibration system composed of a spring, damping, and mass with a certain degree of freedom[33]. To quantify this oscillation, the oscillation frequencies were analyzed in the horizontal ($f_h=1/T_h=\omega_h/2\pi$) and vertical ($f_v=1/T_v=\omega_h/2\pi$) directions using the fast Fourier transform algorithm[50,51] in MATLAB. Under the high Weber numbers, the droplet oscillation frequency was lower than that under the moderate-impact velocity condition, where f_{h50} = 80 Hz < f_{h27} = 93 Hz and f_{vh50} = 76 Hz < f_{v27} = 90 Hz (the frequency of a free-oscillating droplet: f =109 Hz[52]). Thus, the lower frequency and smaller amplitude of the droplet oscillations reveal that more energy is dissipated by the viscous force at high-impact velocities. Additionally, mutations in the degree of freedom of the droplet-spring system due to pinning/depinning can severely inhibit lateral but not vertical droplet oscillations during the retraction process; thus, the lower part of the droplet will again collide with the petal, causing multiple surface energy dissipation as demonstrated in Fig. 7. Artificial SSHSs (e.g., SSHS-1, SSHS-2) are more isotropic with respect to the rose petals but can also become more "hydrophilic" under high Weber numbers. In addition, the underdamped harmonic oscillator, especially in the horizontal direction (Fig. 8a), are highly efficient on the RPS. The pinning effect of the high regimen experienced random oscillation in an underdamped manner on the rose petals. The flatness factor, $\zeta_h = D_h/D_0$, and the dimensionless vertical dimension of the droplet, $\zeta_v = D_v/D_0$, were defined to investigate the degree of oscillation. Furthermore, we analyzed the oscillation phenomenon of the depositional droplet under moderate (W_e =27) and high (W_e =50) Weber numbers as denoted in Fig. 8, resulting in greater damping and droplet stiffness at W_e =50. The increased velocity appeared to attenuate the oscillation amplitude faster than did the collision of a lower velocity droplet on the same petal, indicating a higher effective damping coefficient.

4. Conclusions

There seems to be no consensus on the static petal effects[22–24,26] and a large amount of the previous studies have mainly focused on the wettability of superhydrophobic surfaces[15–21,42].These all determine that the dynamic petal effects are still far from being fully understood yet. We systematically investigated the impact dynamics of droplets on the interfaces of rose petals, imitation rose petals and SHS. Spherical droplet retention is attributed to the sophisticated energy-consuming system at the droplet-petal interface—the ingenious combination of a sticky superhydrophobic texture and an irregular texture. The pinning effect significantly modified the droplets' dynamic wettability. The sticky superhydrophobic surface is a type of superhydrophobic surface with various defects; thus, the above combination effect should be avoided when designing water-repellent surfaces. As we mentioned, the roses may reveal more "hydrophilic" at heavier precipitation. These findings may offer possibilities for designing high-efficiency energy conversion and harvesting[9,10,27].

Conflicts of interest

There are no conflicts of interest to declare.

Acknowledgments

This study was supported by the National Key Research and Development Program of China (Grant No. 2018YFA0703300), the National Natural Science Foundation of China (Grant No. 51575227, 51875243, 51706084), the Science and Technology Development Program of Jilin Province (Grant No. 172411GG010040701) and the Ph.D. Interdisciplinary Research Funding Scheme of Jilin University (Grant No. 10183201828).

Author contributions

C.Z. and Y.Z. conceived the study. Y.Z. and J.W. performed the experiments. J.Y., C.S. and Y.L. performed the simulations. Y.Z. wrote the paper. All the authors analyzed the data, proofread the paper, made comments.

References

[1] M. Nosonovsky, B. Bhushan, Energy transitions in superhydrophobicity: Low adhesion, easy flow and bouncing, J. Phys. Condens. Matter. (2008). doi:10.1088/0953-8984/20/39/395005.

[2] W. Barthlott, C. Neinhuis, Purity of the sacred lotus, or escape from contamination in biological surfaces, Planta. 202 (1997) 1–8.

[3] L. Chen, Z. Xiao, P.C.H. Chan, Y.K. Lee, Z. Li, A comparative study of droplet impact dynamics on a dual-scaled superhydrophobic surface and lotus leaf, Appl. Surf. Sci. 257 (2011) 8857–8863. doi:10.1016/j.apsusc.2011.04.094.

[4] P.-G. de Gennes, F. Brochard-Wyart, D. Quéré, Capillarity and Wetting Phenomena, 2004. doi:10.1007/978-0-387-21656-0.

[5] E. Bormashenko, T. Stein, R. Pogreb, D. Aurbach, “Petal effect” on surfaces based on lycopodium: High-stick surfaces demonstrating high apparent contact angles, J. Phys. Chem. C. (2009). doi:10.1021/jp900594k.

[6] L. Feng, Y. Zhang, J. Xi, Y. Zhu, N. Wang, F. Xia, L. Jiang, Petal effect: A superhydrophobic state with high adhesive force, Langmuir. (2008). doi:10.1021/la703821h.

[7] J.C. Bird, R. Dhiman, H.M. Kwon, K.K. Varanasi, Reducing the contact time of a bouncing drop, Nature. 503 (2013) 385–388. doi:10.1038/nature12740.

[8] J. Li, Z. Jing, F. Zha, Y. Yang, Q. Wang, Z. Lei, Facile spray-coating process for the fabrication of tunable adhesive superhydrophobic surfaces with heterogeneous chemical compositions used for selective transportation of microdroplets with different volumes, ACS Appl. Mater. Interfaces. (2014). doi:10.1021/am5015937.

[9] S. Zhang, J. Huang, Z. Chen, S. Yang, Y. Lai, Liquid mobility on superwettable surfaces for applications in energy and the environment, J. Mater. Chem. A. (2019). doi:10.1039/c8ta09403a.

[10] H. Li, W. Fang, Y. Li, Q. Yang, M. Li, Q. Li, X.-Q. Feng, Y. Song, Spontaneous droplets gyrating via asymmetric self-splitting on heterogeneous surfaces, Nat. Commun. (n.d.) 1–6. doi:10.1038/s41467-019-08919-2.

[11] A.B.D. Cassie, S. Baxter, Wettability of porous surfaces, Trans. Faraday Soc. (1944). doi:10.1039/tf9444000546.

[12] R.N. Wenzel, Resistance of solid surfaces to wetting by water, Ind. Eng. Chem. (1936). doi:10.1021/ie50320a024.

[13] D. Khojasteh, M. Kazerooni, S. Salarian, R. Kamali, Droplet impact on superhydrophobic surfaces: A review of recent developments, J. Ind. Eng. Chem. 42 (2016) 1–14. doi:10.1016/j.jiec.2016.07.027.

[14] C. Neinhuis, W. Barthlott, Characterization and distribution of water-repellent, self-cleaning plant surfaces, Ann. Bot. 79 (1997) 667–677. doi:10.1006/anbo.1997.0400.

[15] J. Lin, Y. Cai, X. Wang, B. Ding, J. Yu, M. Wang, Fabrication of biomimetic superhydrophobic surfaces inspired by lotus leaf and silver ragwort leaf., Nanoscale. 3 (2011) 1258–1262.

[16] T. Verho, C. Bower, P. Andrew, S. Franssila, O. Ikkala, R. RH, Mechanically durable superhydrophobic surfaces., Adv. Mater. 23 (2011) 673–678.

[17] L. Jiang, Y. Zhao, J. Zhai, A lotus-leaf-like superhydrophobic surface: a porous microsphere/nanofiber composite film prepared by electrohydrodynamics., Angew Chem Int Ed

Engl. 43 (2004) 4338–4341.

[18] X.M. Li, D. Reinhoudt, M. Crego-Calama, What do we need for a superhydrophobic surface? A review on the recent progress in the preparation of superhydrophobic surfaces, Cheminform. 36 (2007) 1350–1368.

[19] Q. Sun, H. Liu, T. Chen, Y. Wei, Z. Wei, Facile fabrication of iron-based superhydrophobic surfaces via electric corrosion without bath, Appl. Surf. Sci. 369 (2016) 277–287. doi:10.1016/j.apsusc.2016.02.069.

[20] M. Nosonovsky, B. Bhushan, Hierarchical roughness optimization for biomimetic superhydrophobic surfaces, Ultramicroscopy. 107 (2007) 969–979. doi:10.1016/j.ultramic.2007.04.011.

[21] H. Mertaniemi, R. Forchheimer, O. Ikkala, R.H.A. Ras, Rebounding droplet-droplet collisions on superhydrophobic surfaces: From the phenomenon to droplet logic, Adv. Mater. (2012). doi:10.1002/adma.201202980.

[22] L. Gao, T.J. McCarthy, How Wenzel and Cassie were wrong, Langmuir. 23 (2007) 3762–3765. doi:10.1021/la062634a.

[23] B. Bhushan, E.K. Her, Fabrication of superhydrophobic surfaces with high and low adhesion inspired from rose petal, Langmuir. (2010). doi:10.1021/la904585j.

[24] H. Teisala, M. Tuominen, J. Kuusipalo, Adhesion mechanism of water droplets on hierarchically rough superhydrophobic rose petal surface, J. Nanomater. (2011). doi:10.1155/2011/818707.

[25] S. Yang, J. Du, M. Cao, X. Yao, J. Ju, X. Jin, B. Su, K. Liu, L. Jiang, Direct insight into the three-dimensional internal morphology of solid-liquid-vapor interfaces at microscale, Angew. Chemie - Int. Ed. (2015). doi:10.1002/anie.201411023.

[26] H. Jin, Y. Li, P. Zhang, S. Nie, N. Gao, The investigation of the wetting behavior on the red rose petal, Appl. Phys. Lett. 108 (2016). doi:10.1063/1.4947057.

[27] A.L.L. Yarin, DROP IMPACT DYNAMICS: Splashing, Spreading, Receding, Bouncing…, Annu. Rev. Fluid Mech. 38 (2006) 159–192. doi:10.1146/annurev.fluid.38.050304.092144.

[28] Z. Che, O.K. Matar, Impact of Droplets on Liquid Films in the Presence of Surfactant, Langmuir. 33 (2017) 12140–12148. doi:10.1021/acs.langmuir.7b01901.

[29] C. Shen, C. Zhang, M. Gao, X. Li, Y. Liu, L. Ren, A.S. Moita, Investigation of effects of receding contact angle and energy conversion on numerical prediction of receding of the droplet impact onto hydrophilic and superhydrophilic surfaces, Int. J. Heat Fluid Flow. (2018). doi:10.1016/j.ijheatfluidflow.2018.09.015.
[30] R. Kannan, D. Sivakumar, Drop impact process on a hydrophobic grooved surface, Colloids Surfaces A Physicochem. Eng. Asp. (2008). doi:10.1016/j.colsurfa.2007.12.005.
[31] Y. Liu, L. Moevius, X. Xu, T. Qian, J.M. Yeomans, Z. Wang, Pancake bouncing on superhydrophobic surfaces, Nat. Phys. 10 (2014) 515–519. doi:10.1038/nphys2980.
[32] C. Zhang, Z. Wu, X. Zhang, Y. Yue, J. Wang, Effect of Feather Elasticity of Kingfisher Wing on Droplet Impact Dynamics, J. Bionic Eng. (2018). doi:10.1007/s42235-018-0061-5.
[33] C. Zhang, Y. Zheng, Z. Wu, J. Wang, C. Shen, Y. Liu, L. Ren, Non-wet kingfisher flying in the rain: The water-repellent mechanism of elastic feathers, J. Colloid Interface Sci. 541 (2019) 56–64. doi:10.1016/j.jcis.2019.01.070.
[34] P.B. Weisensee, J. Ma, Y.H. Shin, J. Tian, Y. Chang, W.P. King, N. Miljkovic, Droplet impact on vibrating superhydrophobic surfaces, Phys. Rev. Fluids. 2 (2017) 103601. doi:10.1103/PhysRevFluids.2.103601.
[35] Z. Li, Q. Kong, X. Ma, D. Zang, X. Guan, X. Ren, Dynamic effects and adhesion of water droplet impact on hydrophobic surfaces: bouncing or sticking, Nanoscale. 9 (2017) 8249–8255. doi:10.1039/C7NR02906C.
[36] Y. Shen, J. Tao, Z. Chen, C. Zhu, G. Wang, H. Chen, S. Liu, Rational Design of the Nanostructure Features on Superhydrophobic Surfaces for Enhanced Dynamic Water Repellency, ACS Sustain. Chem. Eng. 6 (2018) 9958–9965. doi:10.1021/acssuschemeng.8b01200.
[37] J. Li, Z. Jing, Y. Yang, L. Yan, F. Zha, Z. Lei, A facile solution immersion process for the fabrication of superhydrophobic ZnO surfaces with tunable water adhesion, Mater. Lett. 108 (2013) 267–269. doi:10.1016/j.matlet.2013.07.024.
[38] L. Moevius, Y. Liu, Z. Wang, J.M. Yeomans, Pancake bouncing: Simulations and theory and experimental verification, Langmuir. 30 (2014) 13021–13032. doi:10.1021/la5033916.
[39] C.M. Pooley, K. Furtado, Eliminating spurious velocities in the free-energy lattice Boltzmann

method, Phys. Rev. E - Stat. Nonlinear, Soft Matter Phys. (2008). doi:10.1103/PhysRevE.77.046702.

[40] B. Bhushan, M. Nosonovsky, The rose petal effect and the modes of superhydrophobicity, Philos. Trans. R. Soc. A Math. Phys. Eng. Sci. (2010). doi:10.1098/rsta.2010.0203.

[41] P.B. Weisensee, J. Tian, N. Miljkovic, W.P. King, Water droplet impact on elastic superhydrophobic surfaces, Sci. Rep. 6 (2016) 1–9. doi:10.1038/srep30328.

[42] R. Gupta, V. Vaikuntanathan, D. Sivakumar, Superhydrophobic qualities of an aluminum surface coated with hydrophobic solution NeverWet, Colloids Surfaces A Physicochem. Eng. Asp. 500 (2016) 45–53. doi:10.1016/j.colsurfa.2016.04.017.

[43] U.U. Ghosh, S. Nair, A. Das, R. Mukherjee, S. DasGupta, Replicating and resolving wetting and adhesion characteristics of a Rose petal, Colloids Surfaces A Physicochem. Eng. Asp. 561 (2019) 9–17. doi:10.1016/j.colsurfa.2018.10.028.

[44] B.A. Malouin, N.A. Koratkar, A.H. Hirsa, Z. Wang, Directed rebounding of droplets by microscale surface roughness gradients, Appl. Phys. Lett. 96 (2010) 94–97. doi:10.1063/1.3442500.

[45] T. Deng, K.K. Varanasi, M. Hsu, N. Bhate, C. Keimel, J. Stein, M. Blohm, Nonwetting of impinging droplets on textured surfaces, Appl. Phys. Lett. 94 (2009) 2–5. doi:10.1063/1.3110054.

[46] A. Alizadeh, V. Bahadur, W. Shang, Y. Zhu, D. Buckley, A. Dhinojwala, M. Sohal, Influence of substrate elasticity on droplet impact dynamics, Langmuir. 29 (2013) 4520–4524. doi:10.1021/la304767t.

[47] M.I. Smith, V. Bertola, Effect of polymer additives on the wetting of impacting droplets, Phys. Rev. Lett. (2010). doi:10.1103/PhysRevLett.104.154502.

[48] D. Zang, X. Wang, X. Geng, Y. Zhang, Y. Chen, Impact dynamics of droplets with silica nanoparticles and polymer additives, Soft Matter. (2013). doi:10.1039/c2sm26759d.

[49] C. Clanet, C. Béguin, D. Richard, D. Quéré, Maximal deformation of an impacting drop, J. Fluid Mech. 517 (2004) 199–208. doi:10.1017/S0022112004000904.

[50] P.D. Welch, The Use of Fast Fourier Transform for the Estimation of Power Spectra: A Method

Based on Time Averaging Over Short, Modified Periodograms, IEEE Trans. Audio Electroacoust. (1967). doi:10.1109/TAU.1967.1161901.

[51] S. Lin, B. Zhao, S. Zou, J. Guo, Z. Wei, L. Chen, Impact of viscous droplets on different wettable surfaces: Impact phenomena, the maximum spreading factor, spreading time and post-impact oscillation, J. Colloid Interface Sci. 516 (2018) 86–97. doi:10.1016/j.jcis.2017.12.086.

[52] L. Chen, Y. Wang, X. Peng, Q. Zhu, K. Zhang, Impact Dynamics of Aqueous Polymer Droplets on Superhydrophobic Surfaces, Macromolecules. 51 (2018) 7817–7827. doi:10.1021/acs.macromol.8b01589.

Dynamic wetting phenomenon on rose petals

Click here to download high resolution image

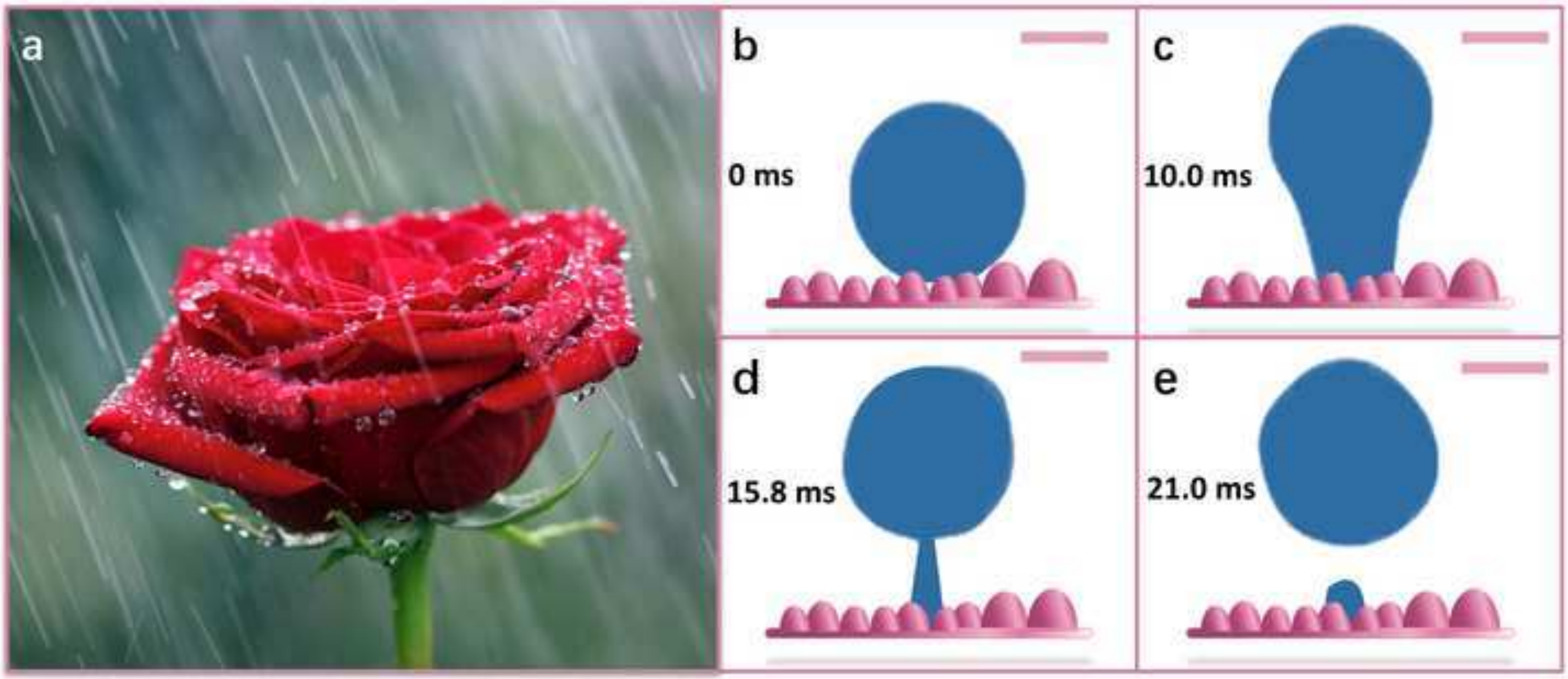

Characterization of the static wettabilities
Click here to download high resolution image

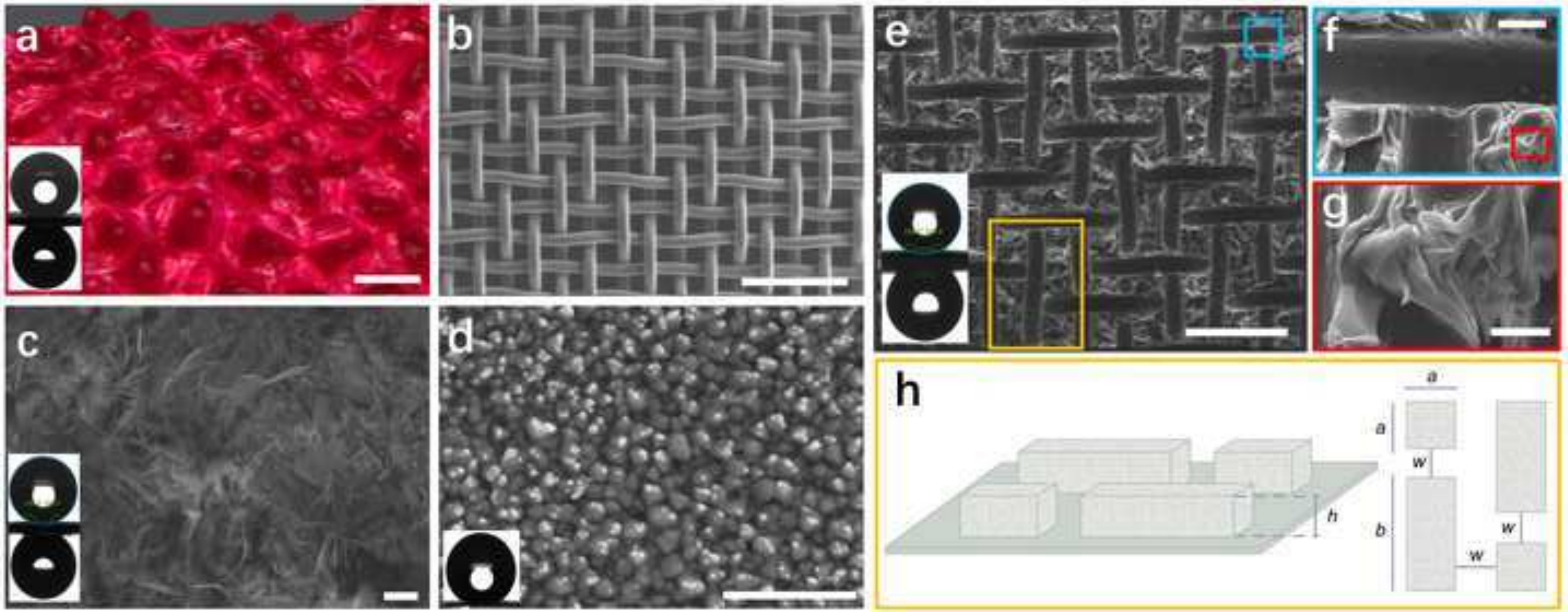

Simulated and experimental analysis and verification

Click here to download high resolution image

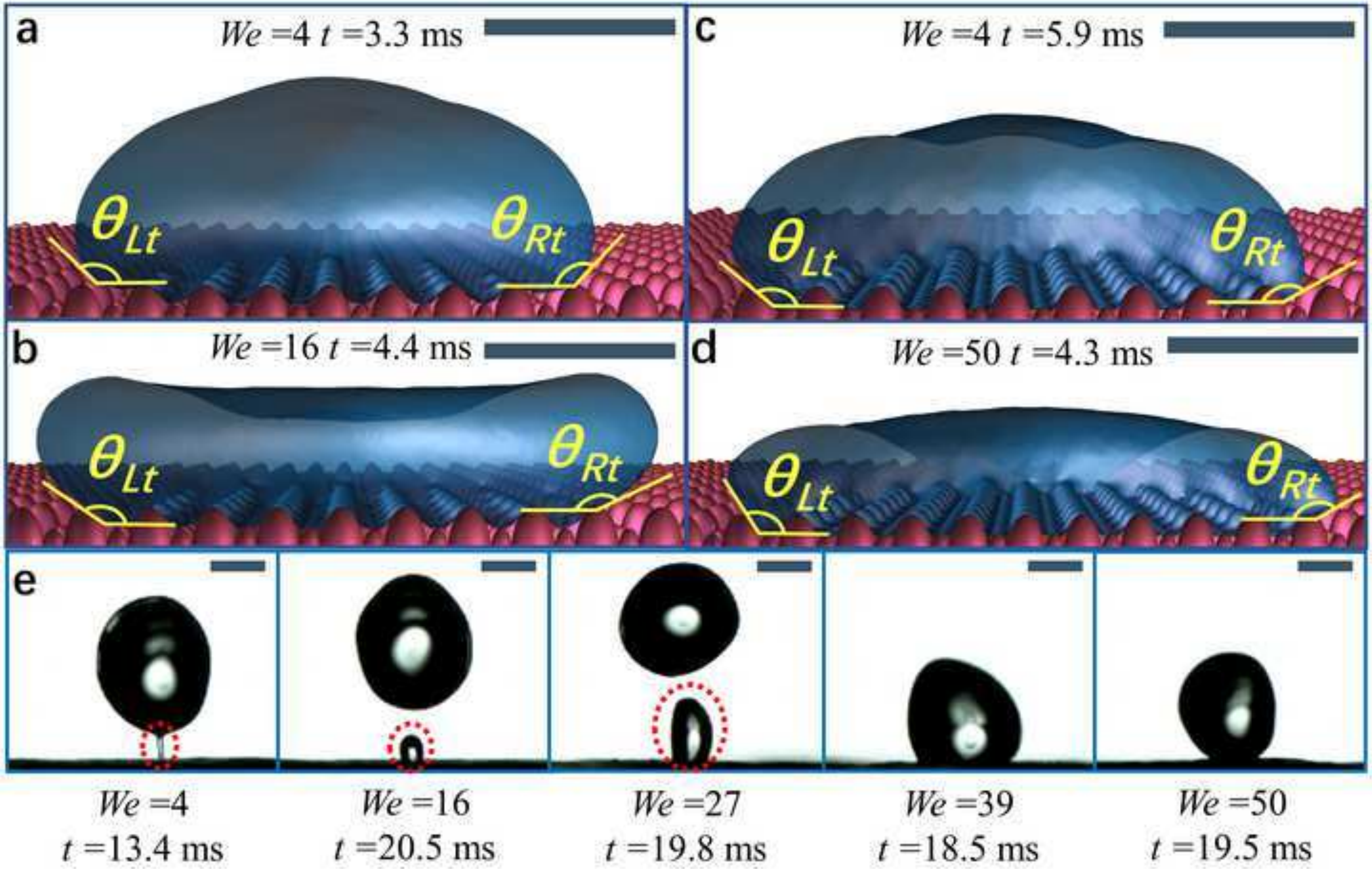

Quantitative and qualitative comparisons

Click here to download high resolution image

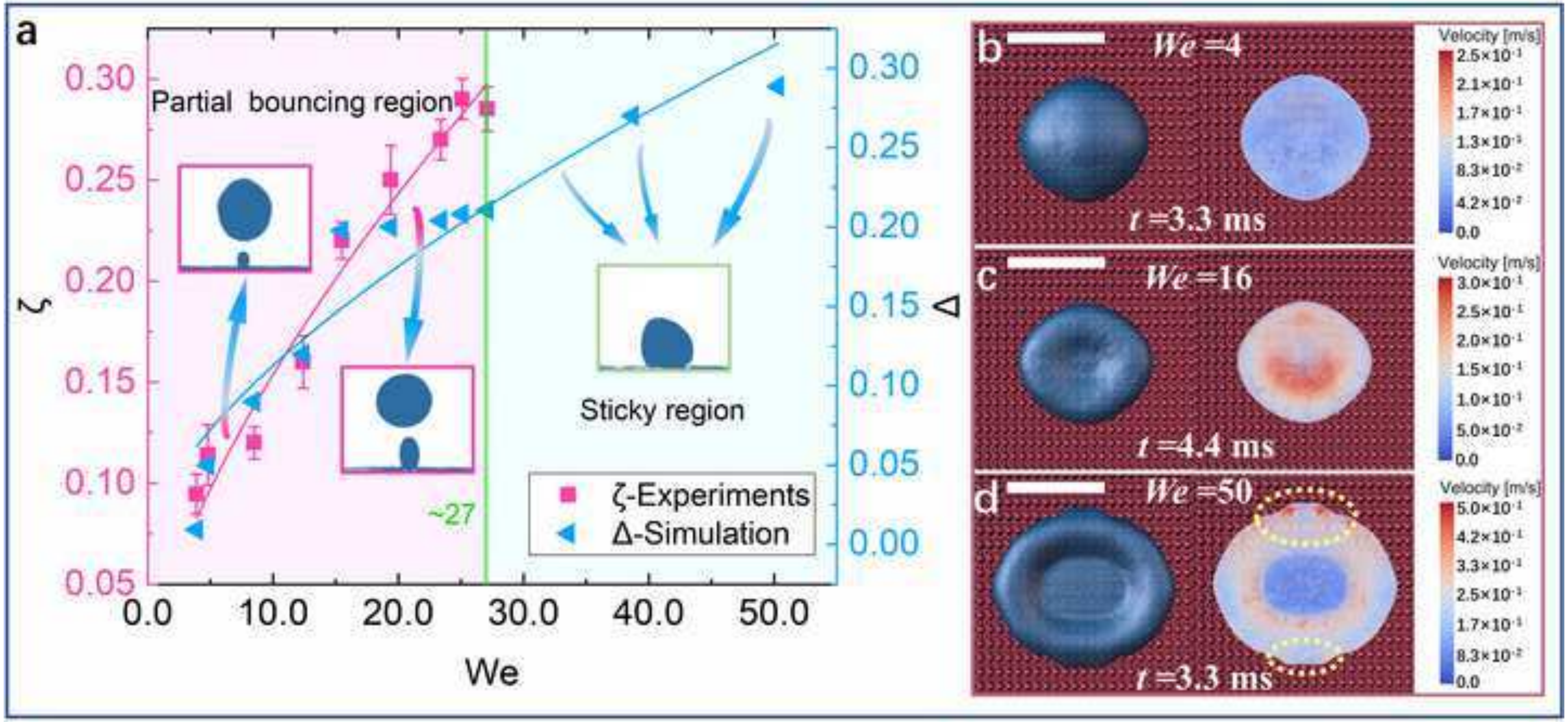

Snapshots of the droplets' dynamic behavior (We= 4)

Click here to download high resolution image

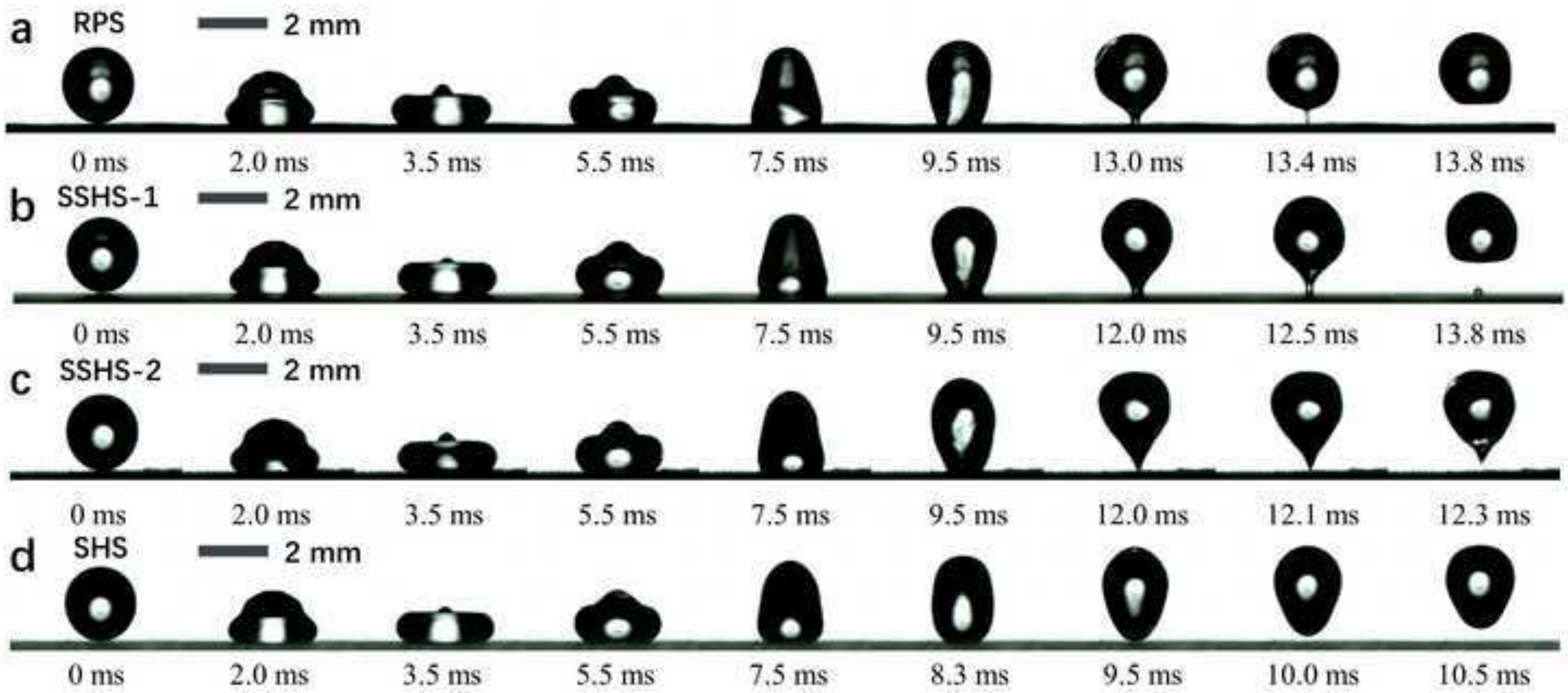

Snapshots of the droplets' dynamic behavior (We= 16)

Click here to download high resolution image

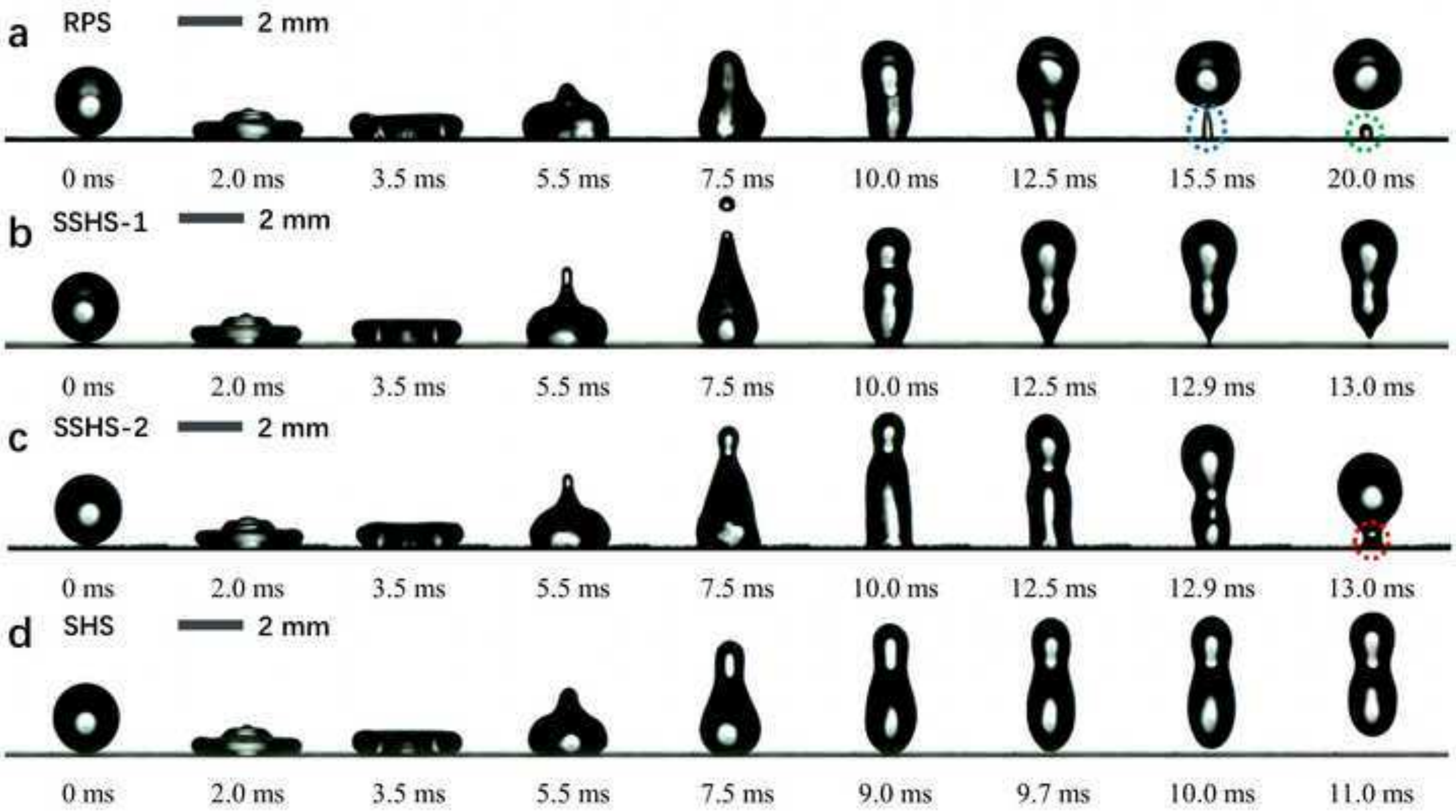

Impact of droplets on the RPS at high velocities

Click here to download high resolution image

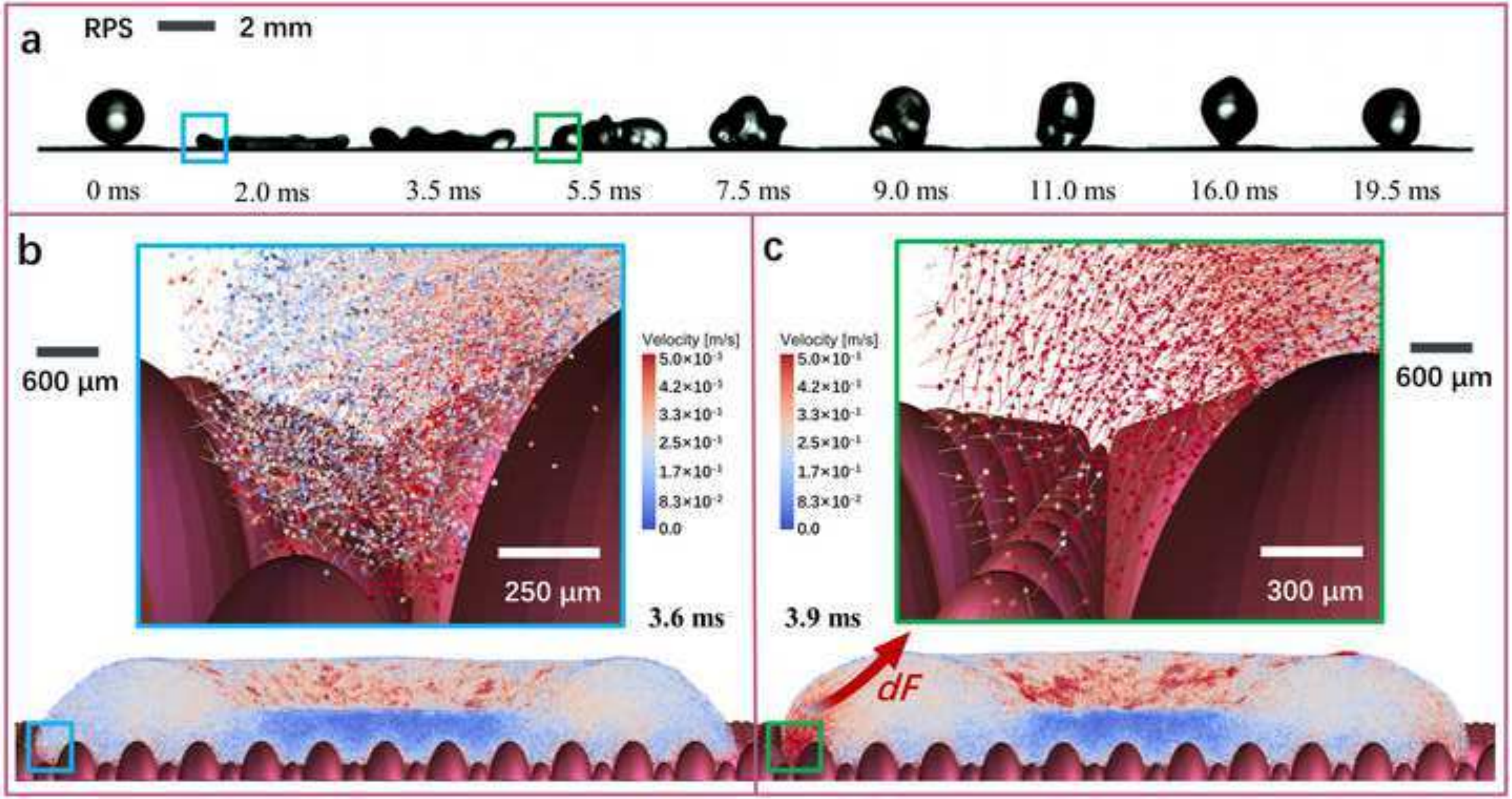

Unique mechanism for suppressing oscillation

Click here to download high resolution image